Draft version May 3, 2022
Typeset using LaTeX **twocolumn** style in AASTeX63

Are there larger stellar velocity dispersions in low redshift Type-1 AGN than in Type-2 AGN?

XueGuang Zhang*[1]

[1]School of Physics and technology, Nanjing Normal University, No. 1, Wenyuan Road, Nanjing, 210023, P. R. China

Submitted to ApJS

ABSTRACT

The main objective is to check the Unified Model (UM) expected similar stellar velocity dispersions between Type-1 AGN and Type-2 AGN, then to provide further clues on BH mass properties. Not similar as previous comparisons of BH masses estimated by $M_{\rm BH}-\sigma$ relations to Type-2 AGN but Virial BH masses in Type-1 AGN, reliable stellar velocity dispersions σ measured through absorption features around 4000Å are directly compared between so-far the largest samples of 6260 low redshift ($z<0.3$) Type-1 AGN and almost all the Type-2 AGN in SDSS DR12. Although half of Type-1 AGN do not have measured σ due to unapparent absorption features overwhelmed by AGN activities, both properties of mean spectra of Type-1 AGN with and without measured σ and positive dependence of σ on [O III] luminosity can lead to statistically larger σ of all the Type-1 AGN than the 6260 Type-1 AGN with measured stellar velocity dispersions. Then, direct σ comparisons can lead to statistically larger σ in Type-1 AGN, with confidence level higher than 10sigma, after considering necessary effects of different redshift and different central AGN activities. Although Type-1 AGN have σ only about (9 ± 3)% larger than Type-2 AGN, the difference cannot be well explained at current stage. Unless there was strong evidence to support different $M_{\rm BH}-\sigma$ relations or to support quite different evolution histories between Type-1 AGN and Type-2 AGN, the statistically larger σ in Type-1 AGN provides a strong challenge to the Unified model of AGN.

Keywords: galaxies:active - galaxies:nuclei - galaxies:absorption lines - galaxies:Seyfert

1. INTRODUCTION

The well-known constantly being revised Unified Model (UM) of AGN (Active Galactic Nuclei) has been widely accepted to explain most of different observational phenomena between broad line AGN (Type-1 AGN) and narrow line AGN (Type-2 AGN), due to effects of different orientation angles of central accretion disk Antonucci (1993), combining with different central activities and different properties of inner dust torus etc. (Marinucci et al. 2012; Oh et al. 2015; Mateos et al. 2016; Balokovic et al. 2018; Brown et al. 2019; Kuraszkiewicz et al. 2021). More recent reviews on the UM can be found in Bianchi et al. (2012) and in Netzer (2015). Considering different viewing angles relative to central dust torus, the UM simply indicates that Type-2 AGN are intrinsically like Type-1 AGN, but Type-2 AGN have their central accretion disk around black hole (BH) and broad line regions (BLRs) seriously obscured by central dust torus, leading to no optical broad line emission features in Type-2 AGN. The simple UM has been strongly supported by clearly detected polarized broad emission lines and/or clearly detected broad infrared emission lines for some Type-2 AGN (Miller & Goodrich 1990; Heisler, Lumsden & Bailey 1997; Tran 2003; Nagao et al. 2004; Onori et al. 2017; Savic et al. 2018; Moran et al. 2020), and the strong resonance of silicate dust at 10μm seen in absorption towards many Type-2 AGN but in emission in Type-1 AGN (Siebenmorgen et al. 2005).

However, even after necessary modifications to the UM, such as different properties of central dust torus and central activities, there are some other challenges to the UM. Franceschini et al. (2002) have supported different evolutionary patterns in Type-1 and Type-2 AGN. Hiner et al. (2009) have shown higher average star formation rates in Type-2 AGN than in Type-1 AGN. More recently, Villarroel & Korn (2014) have shown different neighbours around Type-1 AGN and Type-2 AGN. Zou et al. (2019) have shown that Type-1 AGN tend to have lower stellar masses of host galaxies than Type-2 AGN, through 2463 X-ray selected AGN in the COSMOS field. Bornancini & Garcia Lambas (2020) have

Corresponding author: XueGuang Zhang
xgzhang@njnu.edu.cn

discussed different host galaxy properties, such as UV/optical/IR colours and masses, together with differences in projected galaxy density at small scales (smaller than 100 kpc) and neighbouring galaxy properties, to favour an evolutionary scenario rather than a strict unified model in obscured and unobscured AGN. As detailed discussions in Netzer (2015), the UM has been successfully applied to explain different features between Type-1 and Type-2 AGN in many different ways, however, there are many other features of structures/environments proved to be far from homogeneous among the AGN family.

Based on commonly accepted framework of the UM, BH mass properties could be expected to be similar between Type-1 AGN and Type-2 AGN. As a pioneer work in Netzer (2009), similar BH masses have been found between Type-1 AGN and Type-2 AGN with redshift from 0.1 to 0.2, although the main objective of Netzer (2009) is to check effects of radiation pressure force on gas dynamics in BLRs of AGN. BH masses in Netzer (2009) are estimated by the well-known $M_{\rm BH}-\sigma$ relations (Ferrarese & Merritt 2000; Gebhardt et al. 2000) in Type-2 AGN but by the Virialization assumption (Vestergaard 2002; Peterson et al. 2004; Shen et al. 2011; Rafiee & Hall 2011) applied in Type-1 AGN. However, in recent years, $M_{\rm BH}-\sigma$ relations with much different slopes have been reported in different literature for different samples of objects,

$$\log(\frac{\rm M_{BH}}{\rm M_\odot}) = \alpha + \beta \times \log(\frac{\sigma}{200\ {\rm km\cdot\ s^{-1}}}) \quad (1)$$

The $M_{\rm BH}-\sigma$ relation with $\beta \sim 4$ has been firstly reported in Ferrarese & Merritt (2000); Gebhardt et al. (2000), based on dynamic measured BH masses and stellar velocity dispersions σ of a small sample of nearby quiescent galaxies. More recent reviews of the $M_{\rm BH}-\sigma$ relations can be found in Kormendy & Ho (2013), McConnell & Ma (2013) and Savorgnan & Graham (2015) for samples of quiescent galaxies.

Meanwhile, many studies have reported applications of $M_{\rm BH}-\sigma$ relations from quiescent galaxies to broad line AGN, such as results in Barth et al. (2005); Woo et al. (2013); Ho & Kim (2014); Woo et al. (2015). After well applications of reverberation mapping technique (Blandford & McKee 1982) to determine BLRs sizes (R_{BLRs}, distance between BLRs and central BH) in the sample of reverberation mapped broad line AGN in AGNWATCH project (http://www.astronomy.ohio-state.edu/~agnwatch) (Peterson et al. 2004), Onken et al. (2004) have reported a scaling factor $f \sim 5.5$ required to bring reverberation-based BH masses $M_{BH} = f\,V^2 R_{BLRs}/G$ into agreement with the quiescent galaxy $M_{\rm BH}-\sigma$ relationship. And then, Woo et al. (2010) have reported a virial factor as $f \sim 5.2$ based on an updated reverberation sample including the low-mass local Seyfert 1 galaxies in the Lick AGN Monitoring Project (LAMP) (https://www.physics.uci.edu/~barth/lamp.html) (Bentz et al. 2010; Barth et al. 2015; Williams et al. 2018). Graham et al. (2011) have reported a virial factor as $f \sim 2.8$, based on an updated $M_{\rm BH}-\sigma$ relation of quiescent galaxies and an updated sample of AGN. Park et al. (2012) have shown a preferred virial factor as $f \sim 5.2$ based on a preferred forward statistical estimations. Woo et al. (2015) have reported a virial factor relative to full width at half maximum as broad line width, considering narrow-line Seyfert 1 galaxies. Moreover, considering the reverberation mapped broad line AGN, there are some improved $M_{\rm BH}-\sigma$ relations with much different slopes from 3.25 to 6.34 for different samples of objects listed and discussed in Bennert et al. (2015); Batiste et al. (2017); Zhang et al. (2019); Bennert et al. (2021), which should lead to different BH masses of Type-2 AGN with different $M_{\rm BH}-\sigma$ relations accepted.

Based on the determined virial factors and the well-known R-L empirical relation for BLRs of reverberation mapped broad line AGN as discussed in Kaspi et al. (2000); Bentz et al. (2013), expression on virial BH masses of Type-1 AGN is being improved in common broad line AGN (not only in reverberation mapped broad line AGN), under the Virialization assumptions accepted to broad line emission clouds of central BLRs,

$$\log(\frac{\rm M_{BH}}{\rm M_\odot}) = A + B\log(\frac{\lambda {\rm L_{5100}}}{10^{44}{\rm erg\cdot\ s^{-1}}}) + 2\log(\frac{\rm V}{10^3{\rm km\cdot\ s^{-1}}}) \quad (2)$$

where V represents Kepler velocity of broad line emission clouds which can be traced by broad emission line width, and $B\log(\frac{\lambda {\rm L_{5100}}}{10^{44}{\rm erg\cdot\ s^{-1}}})$ shows hints of distance of BLRs ($R_{\rm BLRs}$) to central BH. Since the empirical R-L relation has been firstly reported by Kaspi et al. (2000) with $B \sim 0.7$ through variabilities of broad Balmer emission lines of the 17 nearby PG quasars, the R-L relation has been modified to $R_{\rm BLRs} \propto \lambda L^{\sim 0.5}$ by more reverberation mapped broad line AGN with necessary corrections of host galaxy contaminations in Bentz et al. (2013). The well accepted $B \sim 0.5$ different from the one used in Netzer (2009) should lead to different BH masses of Type-1 AGN. And moreover, there are different scale factors of A in different literature. Meanwhile, for broad line AGN with measured stellar velocity dispersions, such as the AGN in Bennert et al. (2015), the virial BH masses have large scatters in $M_{\rm BH}-\sigma$ space, leading to large uncertainties on statistical comparisons of virial BH masses of Type-1 AGN under the Virialization assumption and the BH masses of Type-2 AGN by the $M_{\rm BH}-\sigma$ relations.

Moreover, some independent methods have been proposed and applied to estimate central BH mass of individual AGN. Brewer et al. (2011) have presented a direct BH mass measurement in the AGN Arp 151, based on motions of the gas responsible for the broad emission lines. Pancoast et al. (2017) have reported central BH mass measurements that does not

depend upon the virial factor of five Seyfert 1 galaxies from the LAMP 2008 sample, by directly modelling the AGN continuum light curves and the broad Hβ line profiles. And more recently, Williams et al. (2018) have reported central BH mass measurements of seven Seyfert 1 galaxies from the LAMP 2011 sample, by re-constructing dynamic structures of central BLRs. However, the proposed independent method to estimate central BH masses of AGN can not be widely applied in normal AGN with single-epoch spectra.

Different slopes in $M_{\rm BH} - \sigma$ relations and different factors in Virialization assumptions can lead to different properties of estimated BH masses in Type-2 AGN and in Type-1 AGN. It is necessary and interesting to re-check BH mass properties between large samples of Type-1 AGN and Type-2 AGN by different but direct methods, which is the main objective of the manuscript. In the manuscript, rather than the $M_{\rm BH} - \sigma$ relations applied to Type-2 AGN and the Virialization assumptions applied to Type-1 AGN, measured stellar velocity dispersions σ are directly compared between large samples of Type-2 AGN and Type-1 AGN from SDSS DR12 (Sloan Digital Sky Survey, Data Release 12, Alam et al. (2015)). Section 2 presents data samples of Type-1 AGN and Type-2 AGN, methods to measure stellar velocity dispersions through absorption features around 4000Å. Section 3 shows effects of AGN continuum emissions and broad line emissions on our measured stellar velocity dispersions in Type-1 AGN. Section 4 shows reliability of the measured stellar velocity dispersions. Section 5 shows the main results and necessary discussions. Section 6 gives the final summaries and conclusions. And in the manuscript, the cosmological parameters of $H_0 = 70{\rm km\cdot s^{-1}Mpc^{-1}}$, $\Omega_\Lambda = 0.7$ and $\Omega_m = 0.3$ have been adopted.

2. DATA SAMPLES AND METHODS TO MEASURE STELLAR VELOCITY DISPERSIONS

2.1. *Parent samples of Type-1 AGN and Type-2 AGN*

The work is starting from parent samples of Type-1 AGN and Type-2 AGN. Here, only one criterion of redshift smaller than 0.3 ($z < 0.3$) is applied to collect all the low redshift Type-1 AGN from SDSS pipeline classified QSOs (Richards et al. 2002; Ross et al. 2012; Peters et al. 2015; Lyke et al. 2020) in DR12, through the SDSS provided SQL (Structured Query Language) Search tool (http://skyserver.sdss.org/dr12/en/tools/search/sql.aspx) by the following query

```
SELECT plate, fiberid, mjd
FROM SpecObjall
WHERE
    class='QSO' and z<0.30 and zwarning=0
```

where 'SpecObjall' is the SDSS pipeline provided database including basic properties of spectroscopic emission features of emission line galaxies in SDSS DR12. More detailed information of the database 'SpecObjall' can be found in http://skyserver.sdss.org/dr12/en/help/docs/tabledesc.aspx. The SQL query leads 12342 QSOs collected as Type-1 AGN included in the parent sample of Type-1 AGN. And the collected information of plate, fiberid and mjd can be conveniently applied to download SDSS spectra of the 12342 Type-1 AGN.

The same criteria $z < 0.3$ combining with criterion of 'subclass='AGN'' are applied to collect all the low redshift Type-2 AGN from SDSS pipeline classified main galaxies in DR12 by the following query

```
SELECT plate, fiberid, mjd
FROM SpecObjall
WHERE
    class='GALAXY' and z<0.30 and zwarning=0
    and subclass = 'AGN'
```

where 'subclass='AGN'' can be applied to ensure the collected narrow emission line objects well classified as AGN based on the emission line properties. More detailed information of SDSS spectroscopic catalogs can be found in https://www.sdss.org/dr12/spectro/catalogs/. The query above leads 16269 narrow emission line galaxies collected as Type-2 AGN included in the parent sample of Type-2 AGN. Therefore, in the parent samples, there are 12342 Type-1 AGN and 16269 Type-2 AGN.

In the manuscript, high redshift ($z > 0.3$) SDSS AGN are not considered, not only because that it is hard to measure reliable stellar velocity dispersions σ through spectroscopic features of high redshift SDSS AGN, but also because that the SDSS spectra of high redshift AGN will not completely cover the broad Hα emission features which will be applied to determine whether the collected Type-1 AGN have apparent broad emission lines.

2.2. *Method to measure the stellar velocity dispersions*

Stellar velocity dispersions are measured through absorption features within rest wavelength from 3750 to 4600Å described by one broadened template stellar spectrum plus one four-degree polynomial function[1], similar as the direct fitting method proposed and discussed in Rix & White (1992); Barth et al. (2002); Greene & Ho (2006). Meanwhile, when the absorption features are described, the narrow emission lines are being masked out by line width (full width at zero intensity) about 450km s^{-1}, including Hθ, $H\eta$, He Iλ3889Å, Ca H & K, [S II]λ4072Å, Hδ, Hγ and [O III]λ4364Å, the broad emission lines are being masked out by full width at zero intensity about 3000km s^{-1}, especially for the Balmer lines. Here, the 1273 template stellar spectra with high resolution about 30 km $\cdot$ s^{-1} are collected from Indo-U.S. Coude

[1] Higher order polynomial functions have few effects on the final measured velocity dispersions.

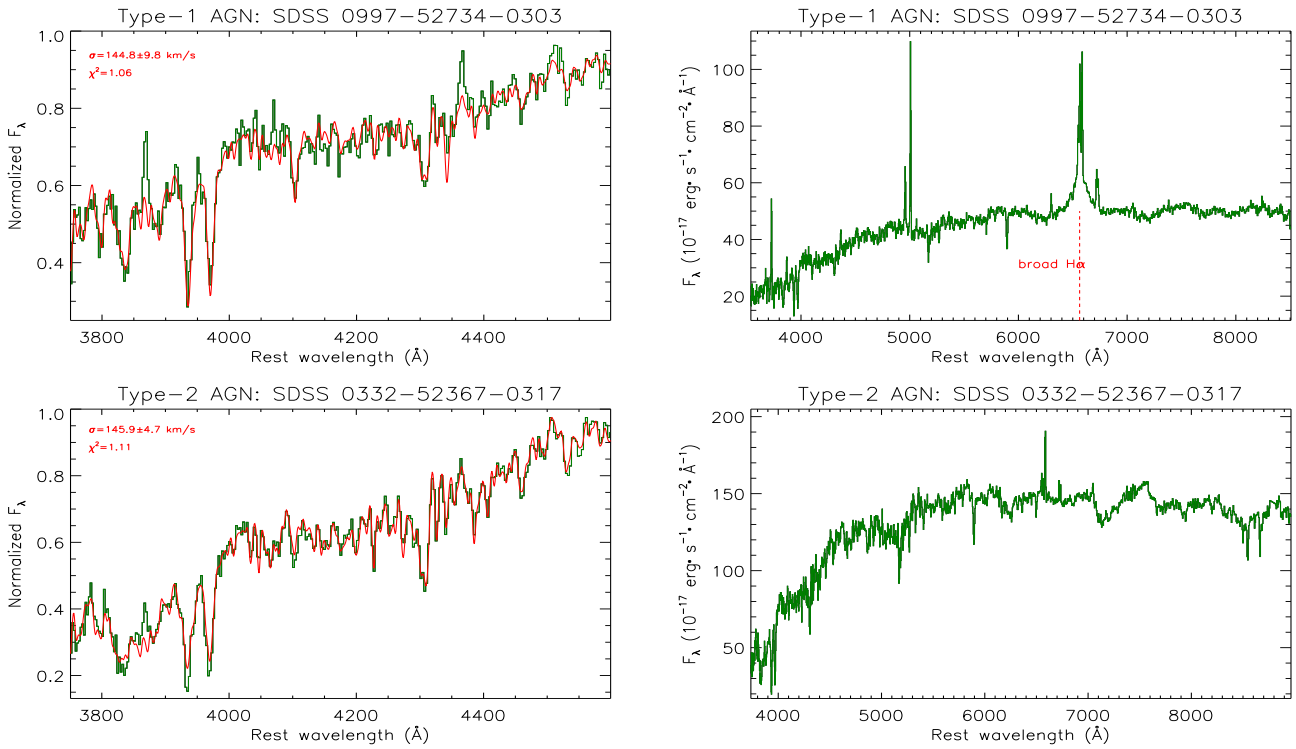

Figure 1. Two examples on the best fitting results (solid red line) to the absorption features around 4000Å (solid dark green line) in Type-1 AGN 0997-52734-0303 (PLATE-MJD-FIBERID) (top panels) and in Type-2 AGN 0332-52367-0317 (bottom panels). In each left panel, the measured stellar velocity dispersion σ and corresponding calculated χ^2 value (summed squared residuals divided by degree of freedom) are marked in top left corner. In right panels, solid dark green lines show the whole observed optical spectrum of the Type-1 AGN 0997-52734-0303 and the Type-2 AGN 0332-52367-0317. The apparent broad Hα is marked in the top-right panel in the Type-1 AGN 0997-52734-0303.

Feed Spectral Library[2] (Valdes et al. 2004). Then, through Levenberg-Marquardt least-squares minimization technique[3], absorption features around 4000Å can be best described by the most appropriate single template stellar spectrum, leading to the well measured stellar velocity dispersions σ and corresponding uncertainties. Because of stronger AGN continuum emissions in SDSS spectra of Type-1 AGN, stellar velocity dispersions can be well measured in about half of the collected Type-1 AGN, but in almost all the Type-2 AGN. Here, we do not show the best fitting results to the absorption features around 4000Å in all the AGN, but Fig. 1 shows two examples, one Type-1 AGN and one Type-2 AGN, on the best fitting results to the absorption features around 4000Å. Among the several methods to measured stellar velocity dispersions (such as the following discussed Simple Stellar Population method), the direct fitting method in the manuscript is mainly considered due to the following reason. Among the Type-1 AGN, absorption features of host galaxies are not apparent in the whole spectra but apparent enough around 4000Å, the direct fitting method applied to the absorption features around 4000Å can lead as many Type-1 AGN as possible with stellar velocity dispersions well measured.

Rather than Ca IIλ8498, 8542, 8662Å triplets and Mg Ib absorption features around 5175Å, the absorption features around 4000Å are mainly considered in the manuscript, due to the following main reasons. On the one hand, for Type-1 AGN in SDSS, only dozens of objects with redshift less than 0.06 have high quality Ca II triplets, leading to a quite small sample of Type-1 AGN of which stellar velocity dispersions can be well measured through Ca II triplets. Moreover, in the following section, it will be confirmed that the measured stellar velocity dispersions are consistent through the Ca II triplets and through the absorption features around 4000Å. On the other hand, not similar as Ca II triplets and absorption features around 4000Å, Mg Ib absorption features in Type-1 AGN have serious contaminations from optical Fe II emissions and prominent Fe I blends. Greene & Ho (2006) have clearly pointed out that the absorption features of the Ca H+K region may provide the only recourse for estimating stellar velocity dispersions, at higher AGN contaminations. Similar discussions can also be found in Harris et al. (2012) which have shown that using Ca H&K instead of CaT seems to be working relatively well.

[2] https://www.noao.edu/cflib/

[3] https://pages.physics.wisc.edu/~craigm/idl/cmpfit.html

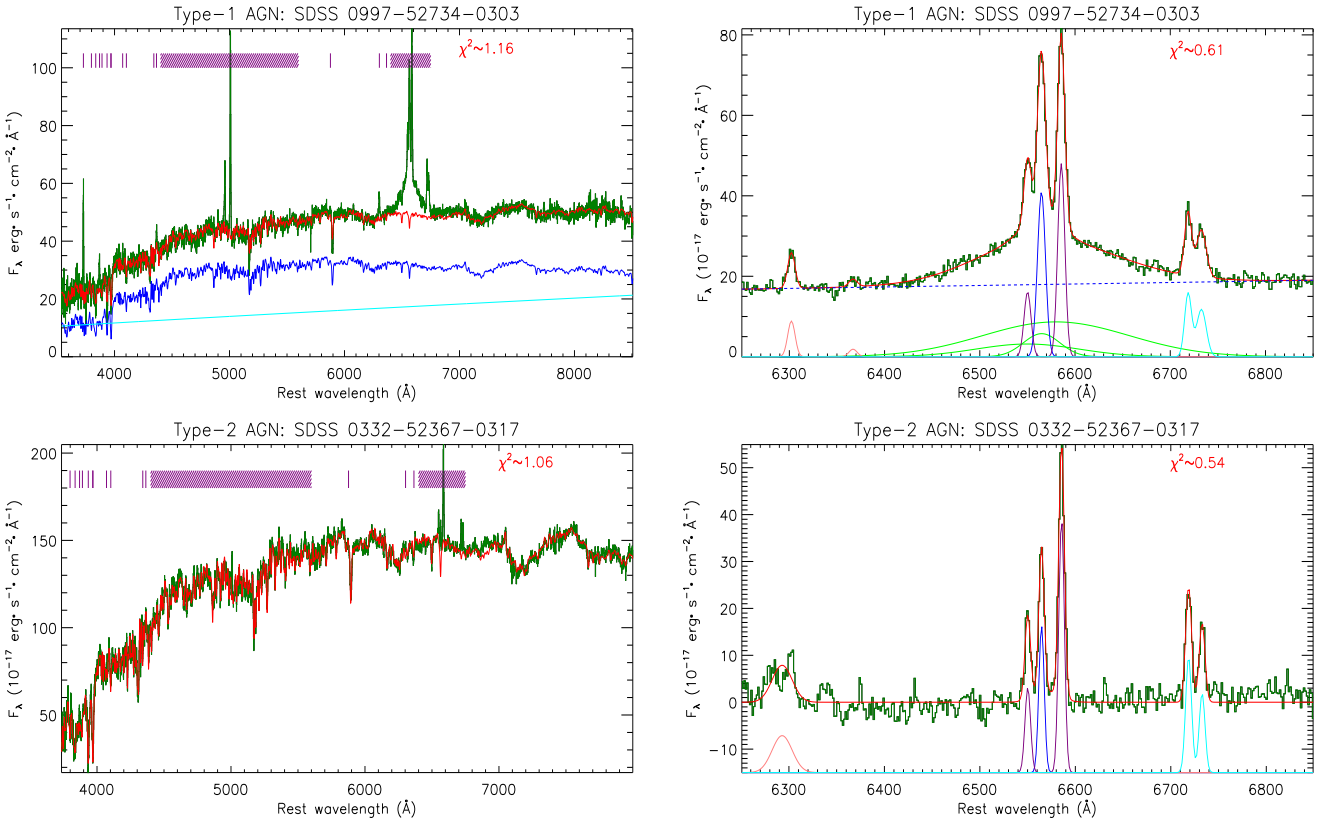

Figure 2. Left panels show the SSP method determined best descriptions (solid red line) to the SDSS spectra (solid dark green line) of Type-1 AGN 0997-52734-0303 and Type-2 AGN 0332-52367-0317 shown in Fig. 1. In each left panel, from left to right, the vertical purple lines point out the emission lines being masked out when the SSP method is running, including [O II]λ3727Å , Hθ, Hη, [Ne III]λ3869Å, He Iλ3891Å, Ca K, [Ne III]λ3968Å, Ca H line, [S II]λ4070Å, Hδ, Hγ, [O III]λ4364Å, He Iλ5877Å and [O I]λ6300, 6363Å doublet, and the area filled by purple lines around 5000Å shows the region masked out including the optical Fe II lines, broad and narrow Hβ and [O III] doublet, and the area filled by purple lines around 6550Å shows the region masked out including the broad and narrow Hα, [N II] and [S II]λ6716Å doublets. In top left panel, solid blue line shows the determined host galaxy contributions, solid cyan line shows the determine AGN continuum emissions in the Type-1 AGN. Right panels show the best descriptions (solid red line) to the emission lines around Hα (solid dark green line) after subtractions of host galaxy contributions. In each right panel, solid blue line shows the determined narrow Hα, solid purple lines show the determine [N II] doublet, solid pink lines show the determined [O I] doublet, solid cyan lines show the determined [S II] doublet. In top right panel, solid green lines show the determined broad Gaussian components in the broad Hα, dashed blue line shows the determined power law continuum emissions underneath the emission lines.

Before proceeding further, it is necessary to ensure broad Balmer emission lines in SDSS spectra of the collected Type-1 AGN but no broad lines in the collected Type-2 AGN. Therefore emission line properties should be further checked after subtractions of host galaxy contributions (if there are). The commonly applied SSP method (Simple Stellar Population) has been applied to determine contributions of host galaxies. The method above to measured stellar velocity dispersions through a single stellar template spectrum is not appropriate to determine host galaxy contributions. More detailed descriptions on the SSP method can be found in Bruzual & Charlot (2003); Kauffmann et al. (2003); Cid Fernandes et al. (2005); Cappellari (2017) and in our previous paper Zhang (2014); Zhang et al. (2016); Rakshit et al. (2017); Zhang et al. (2019, 2021); Zhang (2021a,b). Here, we do not show further detailed discussions on the SSP method any more, but simple descriptions on SSP method as follows. The 39 simple stellar population templates from Bruzual & Charlot (2003) have been exploited, which can be used to well-describe the characteristics of almost all the SDSS galaxies as detailed discussions in Bruzual & Charlot (2003). Meanwhile, there is an additional component, a power law component, which is applied to describe intrinsic AGN continuum emissions, especially when the SSP method is applied to describe spectra of Type-1 AGN. And the power law component is not limited to be blue, because intrinsic host galaxy reddening effects can lead to red power law component, such as the following shown results in the top left panel of Fig. 2 in the Type-1 AGN SDSS 0997-52734-0303. Meanwhile, when the SSP method is applied, the narrow emission lines listed in http://classic.sdss.org/dr1/algorithms/speclinefits.html#linelist are masked out by full width at zero intensity about

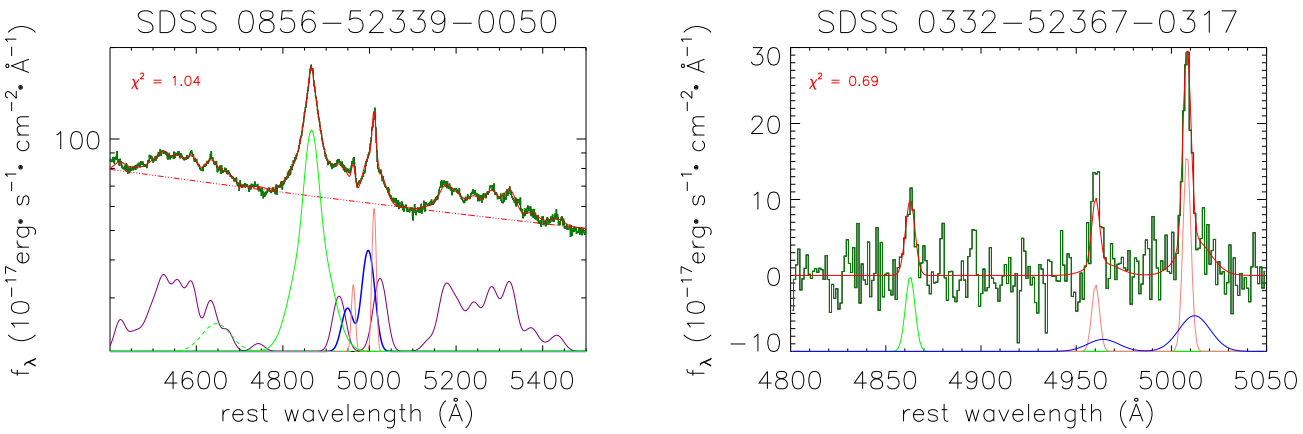

Figure 3. Left panel shows the best fitting results (solid red line) to emission lines around Hβ (solid dark green line) including apparent optical Fe II emission features in the Type-1 AGN 0856-52339-0050. Double-dot-dashed red line shows the determined power law continuum emissions, solid green line shows the determined broad Hβ, solid purple lines show the determined optical Fe II lines, dashed green line shows the determined broad He II line, solid pink lines show the determined core [O III] components, and thick blue solid lines show the determined broad blue-shifted [O III] components. Right panel shows the best fitting results (solid red line) to the emission lines around Hβ (solid dark green line) in the Type-2 AGN 0332-52367-0317 of which SDSS spectrum is shown in Fig. 1 and Fig. 2, after subtractions of host galaxy contributions. Solid green line shows the determined narrow Hβ, solid lines in pink and in blue show the determined core and extended components of [O III] doublet. And the calculated χ^2 values for the best fitting results are marked in the top-left corners in the panels.

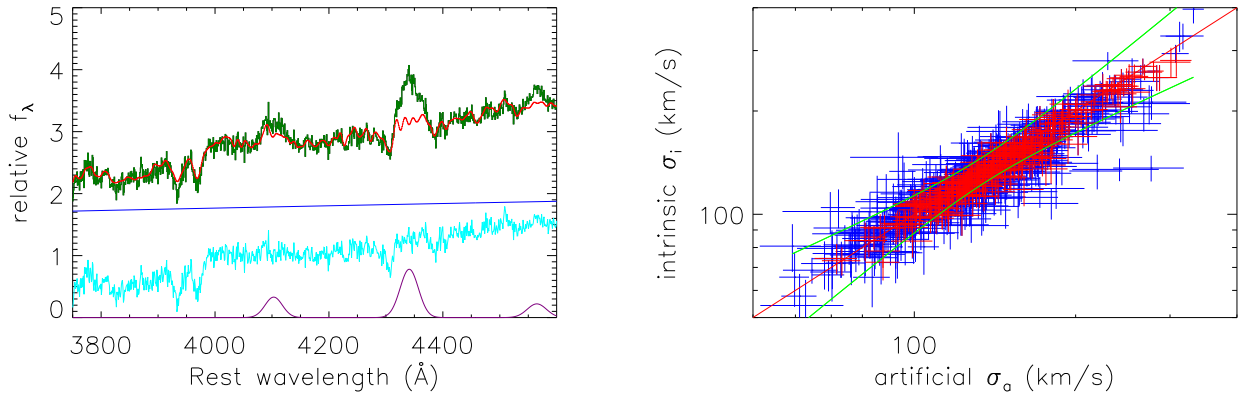

Figure 4. Left panel shows an example of artificial spectrum around 4000Å (solid line in dark green) considering contributions of AGN continuum emissions (solid blue line) and broad line emissions (solid purple lines), and the corresponding best fitting results (solid red line). In left panel, solid cyan line shows the spectrum $S_2(\lambda)$ around 4000Å collected from the Type-2 AGN SDSS 0789-52342-0246. Right panel shows the correlation between intrinsic σ_i and artificial σ_a. In right panel, symbols in blue are for all the data points with artificial σ_a 5 times larger than their corresponding uncertainties, and symbols in red are for the high quality data points with artificial σ_a 10 times larger than their corresponding uncertainties and χ^2 smaller than 2, solid red line shows X=Y, solid green lines show the 99.99% confidence bands to the linear correlation X=Y.

450km s^{-1}, And the wavelength ranges from 4450 to 5600Å and from 6250 to 6750Å are also masked out for the probably broad Hβ and the broad Hα emission lines. Then, through the Levenberg-Marquardt least-squares minimization technique, SDSS spectra with emission lines being masked out can be well described. Here, the SSP method determined host galaxy contributions are not shown in plots for all the AGN, but for the two AGN shown in Fig. 1, the SSP determined host galaxy contributions are shown in left panels of Fig. 2.

After subtractions of host galaxy contributions (if there are), emission lines around Hα within rest wavelength from 6250 to 6850Å can be carefully measured, in order to check whether there are broad Hα emission lines. To measure properties of emission lines are not the objective of the manuscript, but simple descriptions are as follows on the emission line fitting procedure. Similar as what we have recently done in Zhang

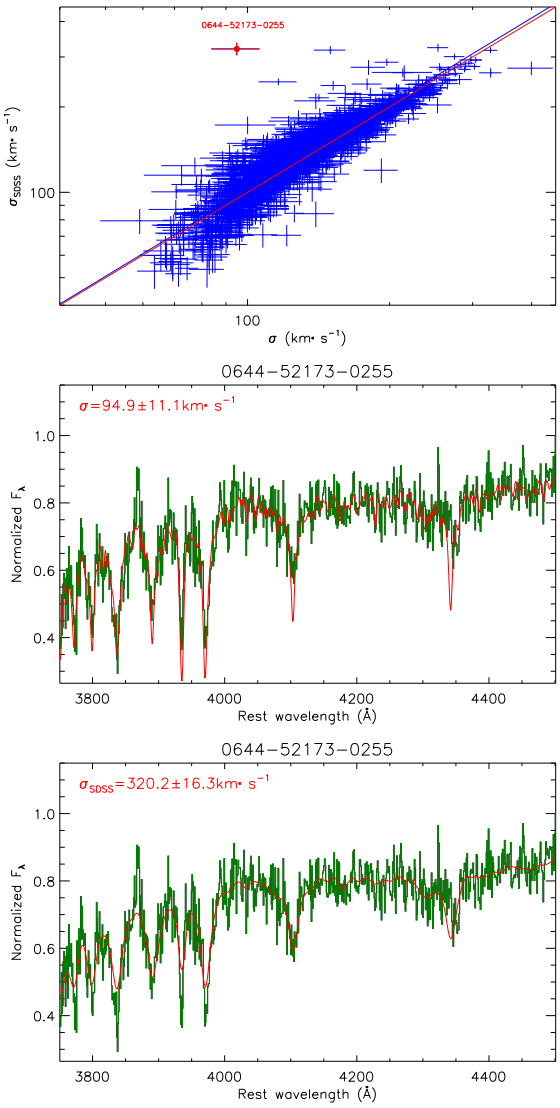

Figure 5. Top panel shows the correlation between the measured stellar velocity dispersions σ and the SDSS pipeline provided $\sigma_{\rm SDSS}$ for the Type-2 AGN. Solid blue line shows the best fitting results, and solid red line shows $\sigma = \sigma_{\rm SDSS}$. Middle and bottom panel show the best fitting results to the absorption features around 4000Å by the fitting procedure in the manuscript with $\sigma \sim$ 95km/s, and the fitting results to the absorption features around 4000Å with stellar velocity dispersion fixed to the SDSS pipeline provided 320km/s.

(2021a,b,c), three broad Gaussian functions (second moment larger than 600km $\cdot$ s^{-2}) are applied to describe broad Hα, and seven narrow Gaussian components (second moment smaller than 600km $\cdot$ s^{-2}) are applied to describe narrow Hα, [O I], [N II] and [S II] doublets, and a power law component is applied to describe continuum emissions underneath broad Hα. Based on the measured parameters of broad Hα through the Levenberg-Marquardt least-squares minimization technique, the criteria are accepted to determine that there are no broad Hα: the determined three broad Gaussian components for broad Hα with the measured line fluxes and line widths 2 times smaller than the corresponding uncertainties, and the criteria are accept to determine that there are reliable broad Hα: there are at least one broad Gaussian component with measured line flux and line width at least 5 times larger than their corresponding uncertainties and second moment larger than 600km $\cdot$ s^{-1}. The best descriptions to the emission lines around Hα are not shown in plots for all the AGN, but for the two AGN shown in Fig. 1, the best descriptions to the emission lines around Hα are shown in right panels of Fig. 2.

Furthermore, emission line properties of [O III] line should be applied in the manuscript. Therefore, simple descriptions are shown on the model functions to describe emission lines around Hβ within rest wavelength from 4400 to 5600Å after subtractions of host galaxy contributions. Similar as what we have recently done in Zhang (2021a,b,c), three broad Gaussian functions are applied to describe broad Hβ, one narrow Gaussian component is applied to describe narrow Hβ, two narrow and two broad Gaussian components are applied to describe core and extended components of [O III]λ4959, 5007Å doublet, one Gaussian component is applied to describe He II line, broadened and scaled Fe II templates discussed in Kovacevic et al. (2010) are applied to describe probable optical Fe II lines, and a power law component is applied to describe continuum emissions underneath broad Hβ. Fig. 3 shows two examples on the best-fitting results to emission lines around Hβ through the Levenberg-Marquardt least-squares minimization technique.

Finally, based on the following criteria,

- The measured stellar velocity dispersions are at least 5 times larger than their corresponding uncertainties.
- The measured stellar velocity dispersions are larger than 50 km $\cdot$ s^{-1} and smaller than 400 km $\cdot$ s^{-1}.
- The χ^2 should be smaller than 2, based on the best fitting results to the absorption features around 4000Å.
- For the Type-1 AGN, there are reliable broad emission lines with at least one broad Gaussian component with the measured line flux and line width at least 5 times larger than the corresponding uncertainties and second moment larger than 600km $\cdot$ s^{-1}.
- For the Type-2 AGN, there are no broad emission lines with the determined three broad Gaussian components for broad Hα with the measured line fluxes and line widths 2 times smaller than the corresponding uncertainties.

there are 6260 Type-1 AGN with apparent broad Hα emission lines and reliable stellar velocity dispersions, and 15353 Type-2 AGN with reliable stellar velocity dispersions but no broad

Hα emission lines. And the sample of the 6260 Type-1 AGN is so far the largest sample of Type-1 AGN with reliable measured stellar velocity dispersions, about 85 times larger than the more recent sample of Type-1 AGN with measured stellar velocity dispersions in Bennert et al. (2015, 2021). And through absorption features around 4000Å, there are 50.7% (6260 of 12342) of Type-1 AGN with stellar velocity dispersions well measured, and 94.4% (15353 of 16269) of Type-2 AGN with stellar velocity dispersions well measured.

The necessary parameters of all the 6260 Type-1 AGN and all the 15353 Type-2 AGN are not listed in the manuscript, but can be downloaded from https://pan.baidu.com/s/1NCDqFtJwRaG-u21ekxlvvQ with validation code sj6f. There are 11 columns in the data file of type1_vd.list and type2_vd.list in ASCII format for the 6260 Type-1 AGN and the 15353 Type-2 AGN with information of SDSS PLATE-MJD-FIBERID, measured σ and uncertainty in unit of km $\cdot$ s^{-1} without corrections of instrument resolutions, χ^2 value for the best fitting results to the absorption features around 4000Å, redshift, logarithmic line luminosity and uncertainty of total [O III] line in unit of erg $\cdot$ s^{-1}, logarithmic line luminosity and uncertainty of core component of [O III] line in unit of erg $\cdot$ s^{-1}, logarithmic ratio of O3HB (flux ratio of core component of [O III]λ5007Å to narrow Hβ), logarithmic ratio of N2HA (flux ratio of [N II]λ6583Å to narrow Hα).

3. TO CONFIRMED FEW EFFECTS OF AGN ACTIVITIES ON THE MEASURED STELLAR VELOCITY DISPERSIONS IN TYPE-1 AGN

Before proceeding further, it is necessary to check effects of AGN activities, especially power law AGN continuum emissions and broad line emissions, on our measured stellar velocity dispersions through absorption features around 4000Å by the fitting procedure described in the Section above, due to apparent AGN continuum emissions and broad line emissions in Type-1 AGN. In the section, series of artificial spectra are created including different contributions of AGN continuum emissions and broad emission lines, and then to check whether are there apparent effects of continuum emissions or broad line emissions on the measured stellar velocity dispersions in Type-1 AGN.

Based on SDSS spectra $S_2(\lambda)$ of Type-2 AGN with well measured stellar velocity dispersions, artificial spectra $S_a(\lambda)$ can be created with contributions of AGN continuum emissions $P_{AGN}(\lambda)$ and broad line emissions $L_{br}(\lambda)$,

$$\begin{aligned} S_a(\lambda) &= S_2(\lambda) + P_{AGN}(\lambda) + L_{br}(\lambda) \\ &= S_2(\lambda) + C_0 \times (\frac{\lambda}{5100\text{Å}})^{\alpha} \\ &+ \sum_{i=1}^{3} Gauss1(\lambda, [\lambda_{0,i}, \sigma_0, f_{0,i}]) \end{aligned} \quad (3)$$

where $P_{AGN}(\lambda) = C_0 \times (\frac{\lambda}{5100\text{Å}})^{\alpha}$ means AGN continuum emissions, $L_{br}(\lambda) = \sum_{i=1}^{3} Gauss1(\lambda, [\lambda_{0,i}, \sigma_{0,i}, f_{0,i}])$ means Gaussian like broad emission lines. For AGN continuum emissions, α is randomly selected from -2 to 0.5, as well discussed results on composite spectrum of SDSS QSOs in Vanden Berk et al. (2001). And for broad emission lines within rest wavelength range from 3750Å to 4600Å, the three broad lines of Hδ ($\lambda_{0,1}$ = 4103Å), Hγ ($\lambda_{0,2}$ = 4341Å) and the broad optical Fe II (opt37, opt38, $\lambda_{0,3} \sim$ 4565Å) are mainly considered. The other broad line features (such as Hϵ and the other optical Fe II features) within rest wavelength from 3750 to 4600Å are not considered, because they are quite weak. Flux ratios of the three broad line features ($f_{0,1}$ as line flux of broad Hδ, $f_{0,2}$ as line flux of broad Hγ, $f_{0,3}$ as line flux of the optical Fe II feature) are accepted as $f_{0,1} : f_{0,2} : f_{0:3} = 5.05 : 12.62 : 3.76$ from the composite spectrum of SDSS QSOs. The same second moments from 600 to 2000km/s are accepted to the three broad line features. Accepted the strong correlation between continuum luminosity at 5100Å and the Hβ luminosity in Greene & Ho (2005b) and based on the reported continuum luminosity and broad Hβ luminosity of the quasars in SDSS DR7 in Shen et al. (2011), the input values of C_0 and $f_{0,2}$ are tied to be

$$\frac{3.3 \times f_{0,2}}{10^{-17}\text{erg/s/cm}^2} \sim 51 \times \frac{C_0}{10^{-17}\text{erg/s/cm}^2/\text{Å}} \quad (4)$$

where the factor 3.3 is the flux ratio of Hβ to Hγ.

Based on randomly selected C_0 from 0.2 to 10 times of the mean intensity of $S_2(\lambda)$, α randomly selected from -2 to 0.5 and σ_0 randomly selected from 600 to 2000km/s and randomly collected $S_2(\lambda)$ among the 11353 Type-2 AGN, 1000 artificial spectra are created with contributions of both AGN continuum emissions and broad line emissions. If there were apparent effects of AGN activities on the measured stellar velocity dispersions, re-measured stellar velocity dispersions σ_a in $S_a(\lambda)$ should be quite different from the stellar velocity dispersions σ_i in $S_2(\lambda)$ of Type-2 AGN. Left panel of Fig. 4 shows an example of $S_a(\lambda)$ and the best fitting results to the absorption features in the artificial spectrum. Right panel of Fig. 4 shows the correlation between artificial σ_a and intrinsic σ_i of the 628 artificial spectra with measured σ_a five times larger than corresponding uncertainties. There are no reliable measured stellar velocity dispersions in the other 372 artificial spectra which have the mean C_0 about two times higher than the C_0 applied in the 628 artificial spectra with reliable measured stellar velocity dispersions, due to their measured σ_a three times smaller than their corresponding uncertainties. There is a strong positive linear correlation with Spearman Rank correlation coefficient about 0.92 with $P_{null} < 10^{-10}$ for the results shown in right panel of Fig. 4. Under considerations of uncertainties in both coordinates, the correlation

can be described by

$$\log(\frac{\sigma_i}{\mathrm{km/s}}) = (-0.046\pm0.047) + (0.976\pm0.022)\times\log(\frac{\sigma_a}{\mathrm{km/s}}) \quad (5)$$

through the FITEXY code (https://idlastro.gsfc.nasa.gov/ftp/pro/math/fitexy.pro written by Frank Varosi) (Tremaine et al. 2002). Meanwhile, the mean ratio of artificial σ_a to intrinsic σ_i is about 1.04±0.03, with the uncertainty 0.03 estimated through the bootstrap method with 1000 loops. For each loop, a new sample of $\sigma_{a,pos}/\sigma_{i,pos}$ is created with more than half data points randomly collected from the sample of σ_a/σ_i. After 1000 loops, there are 1000 new samples with 1000 mean values, the half width at half maximum of distribution of the 1000 mean values is accepted as the uncertainty of the mean value of σ_a/σ_i.

Moreover, the mean ratio 1.04 of artificial σ_a to intrinsic σ_i kindly larger than 1 apparently indicates central AGN continuum emissions and/or broad emission lines can lead the measured stellar velocity dispersions to be about 4% larger than the intrinsic values in Type-1 AGN. In order to confirm the mean ratio of artificial σ_a to intrinsic σ_i, one another sample of 1000 artificial spectra are created. The totally same mean ratio 1.04 can be found in the new sample of 1000 artificial spectra. Therefore, the mean ratio of artificial σ_a to intrinsic σ_i about 1.04 is intrinsically true, due to effects of central AGN continuum emissions and/or broad emission lines.

Before the end of the section, one point is noted. In right panel of Fig. 4, there are some outliers. However, there is only one criterion collect artificial σ_a that σ_a at least 5 times larger than their corresponding uncertainties. If firm criteria are applied that χ^2 smaller than 2 (the critical value applied in Section 2) and σ_a at least 10 times larger than their corresponding uncertainties, the collected 262 data points marked as red symbols are well lying within 99.99% confidence bands of the linear correlation $Y = X$. Moreover, the mean ratio of artificial σ_a to intrinsic σ_i of the 262 high quality data points is about 1.038 totally similar as the 1.04 for all the data points. Therefore, the outliers are only due to rough selection criteria, and there are no further discussions on the outliers in the Fig. 4 which have few effects on our final results.

Contributions of AGN continuum emissions and broad line emissions have apparent effects on measuring stellar velocity dispersions in the Type-1 AGN, the effects can lead to unmeasured stellar velocity dispersions in the Type-1 AGN with strong AGN continuum emissions, meanwhile, the effects can lead the measured reliable stellar velocity dispersions in the Type-1 AGN to be about 4% larger than their intrinsic values, which will be carefully discussed in the following stellar velocity dispersion comparisons between Type-2 AGN and Type-1 AGN.

4. TO CONFIRM THE RELIABILITY OF THE MEASURED STELLAR VELOCITY DISPERSIONS

The main objective of the section is to provide evidence to confirm/support the reliability of our measured stellar velocity dispersions in Type-2 AGN and in Type-1 AGN, by comparing our measured values and reported values in the literature.

For Type-2 AGN, the measured σ are compared with SDSS provided values σ_{SDSS}, shown in top panel of Fig. 5. The SDSS pipeline determined σ_{SDSS} are based on the 24 broadened template eigen-spectra from the ELODIE stellar library well discussed in Prugniel & Soubiran (2001) applied to describe the whole host galaxy absorption features in SDSS spectra, through the similar minimum least-squares minimization technique. More discussions on the SDSS pipeline determined σ_{SDSS} can be found in Shu et al. (2012); Thomas et al. (2013). More detailed information of the SDSS pipeline determined σ_{SDSS} can be found in https://www.sdss.org/dr12/algorithms/redshifts/. More recently, Woo et al. (2016) have compared the SDSS pipeline provided stellar velocity dispersions with the [O III] line width on studying properties of outflows in Type-2 AGN.

Between the measured σ and the σ_{SDSS}, there is one strong linear correlation with Spearman Rank correlation coefficient of 0.92 with $P_{null} < 10^{-10}$. Under considerations of uncertainties in both coordinates, the correlation can be described by

$$\log(\frac{\sigma_{\mathrm{SDSS}}}{\mathrm{km\cdot\ s^{-1}}}) = (-0.01\pm0.01) + (1.01\pm0.05)\times\log(\frac{\sigma}{\mathrm{km\cdot\ s^{-1}}}) \quad (6)$$

through the FITEXY code. The mean ratio of σ to σ_{SDSS} is about 0.985±0.003, with the uncertainty 0.003 estimated by the bootstrap method with 1000 loops. The strong linear correlation and the mean ratio of σ to σ_{SDSS} near to 1 clearly indicate that the measured σ through absorption features around 4000Å are reliable enough for the Type-2 AGN.

Although there is a strong linear correlation in Fig. 5, there are some outliers in the space of σ versus σ_{SDSS}, such as the extreme outlier SDSS 0644-52173-0255 which has $\sigma \sim 95$km/s measured through absorption features around 4000Å in the manuscript however $\sigma_{SDSS} \sim 320$km/s in SDSS database. The best fitting results to the absorption features around 4000Å are shown in middle panel of Fig. 5 with $\chi^2 \sim 1.02$. And in order to show further clues to support our measured stellar velocity dispersion in SDSS 0644-52173-0255, bottom panel of Fig. 5 shows the fitting results to the absorption features around 4000Å with stellar velocity dispersion fixed to the SDSS pipeline provided $\sigma_{SDSS} \sim 320$km/s, leading to bad fitting results to the absorption features with rest wavelength from 3800Å to 4000Å, indicating stellar velocity dispersion around 320km/s not preferred in SDSS 0644-52173-0255. We do not know the exact reason leading to so large SDSS pipeline determined stellar velocity dis-

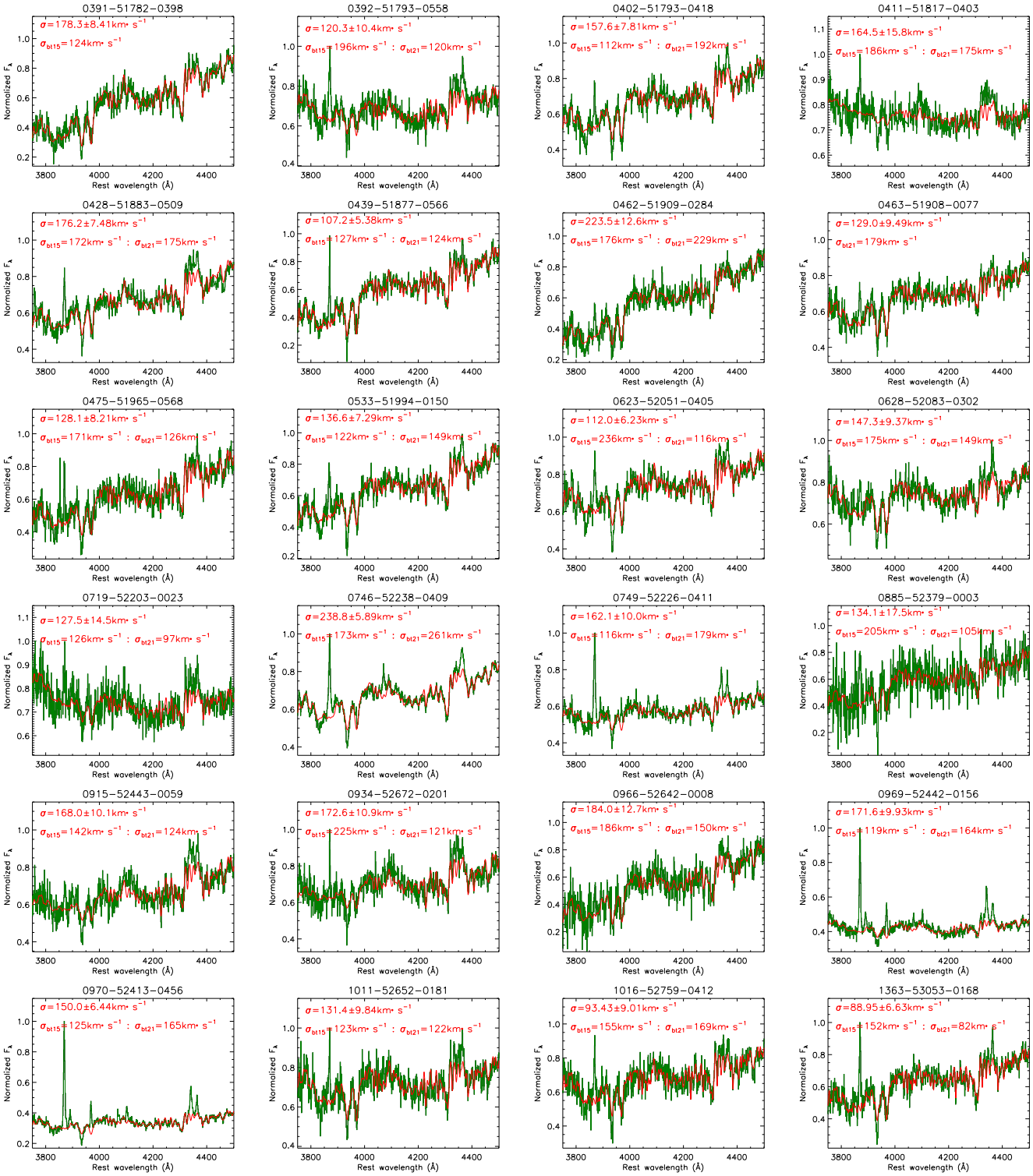

Figure 6. Best fitting results (solid red line) to the absorption features around 4000Å (solid dark green line) of the 41 Type-1 AGN included in the sample of Bennert et al. (2015) and in the sample of Bennert et al. (2021), and the 2 Type-1 AGN from the sample of Xiao et al. (2011) and 5 Type-1 AGN from the sample of Harris et al. (2012). The measured stellar velocity dispersion σ in the manuscript after corrections of instrument resolutions and the reported value σ_{bt15} in Bennert et al. (2015) and/or σ_{bt21} in Bennert et al. (2021), or σ_{xb11} in Xiao et al. (2011), or σ_{hb12} in Harris et al. (2012) are marked in red characters in each panel.

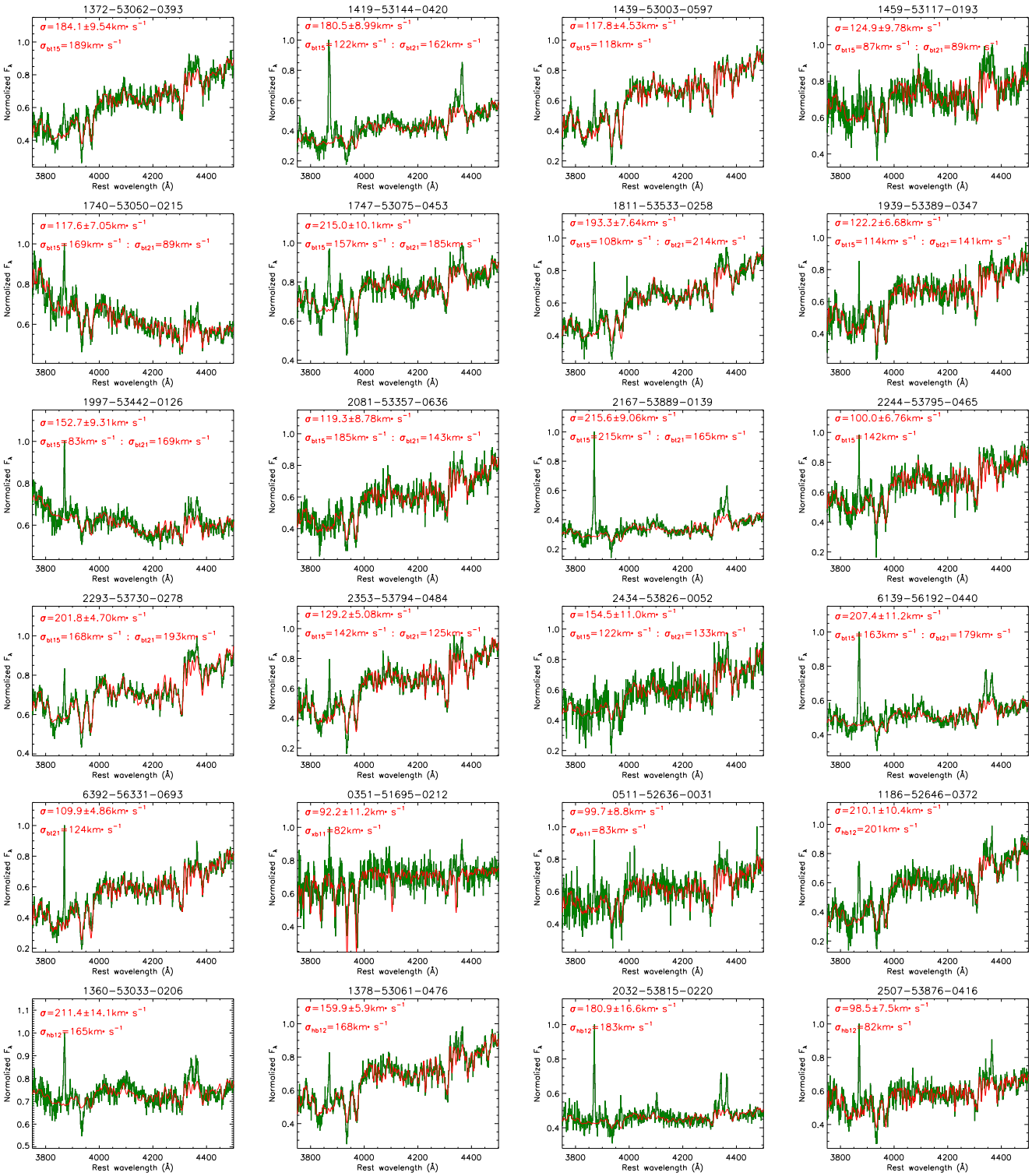

Figure 6. –to be continued

persion in SDSS 0644-52173-0255, but probably due to the following main reason that the SDSS pipeline provided stellar velocity dispersion is measured through the whole host galaxy absorption features including more contaminations. We do not have an idea to determine how many outliers in the space of σ versus $\sigma_{\rm SDSS}$, however the strong linear correlation and the mean ratio of σ to $\sigma_{\rm SDSS}$ being well near to 1 can be applied as strong statistical evidence to support the reliability of our measured stellar velocity dispersions in the Type-2 AGN.

There are no $\sigma_{\rm SDSS}$ provided by SDSS for Type-1 AGN, but the following three methods are applied to confirm the reliability of the measured σ in Type-1 AGN. First, it can be applied to confirm the reliability of our measured stellar velocity dispersions in Type-1 AGN, by comparing our measured values and the more confident spatially resolved values in Bennert et al. (2015, 2021). The spatially-resolved stellar velocity dispersion measurements from Keck long-slit spectra in Bennert et al. (2015, 2021) have more advantages in the measurements than relying only on fiber-based SDSS spectra. There are 65 Type-1 AGN included in the sample of Bennert et al. (2015) with measurements of stellar velocity dispersions derived for both aperture and spatially resolved spectra, and 66 Type-1 AGN in the sample of Bennert et al. (2021) (63 Type-1 AGN included in the sample of Bennert et al. (2015) and 3 new Type-1 AGN) with determined stellar velocity dispersions from spatially resolved measurements integrated within effective spheroid radius. Among the 65 Type-1 AGN in Bennert et al. (2015) and the 66 Type-1 AGN in Bennert et al. (2021), there are 41 AGN of which σ can be well measured through absorption features around 4000Å. Among the 41 Type-1 AGN, 2 Type-1 AGN is firstly reported in the sample of Bennert et al. (2021), 4 Type-1 AGN are only reported in the sample of Bennert et al. (2015), the other 35 Type-1 AGN are reported both in the sample of Bennert et al. (2015) and in the sample of Bennert et al. (2021). The best fitting results to the absorption features around 4000Å are shown in Fig. 6 for the 41 Type-1 AGN, with the measured stellar velocity dispersions σ in the manuscript and the reported stellar velocity dispersions σ_{bt15} in Bennert et al. (2015) and σ_{bt21} in Bennert et al. (2021) marked in each panel of Fig. 6 (the velocity dispersions are not listed in a table any more).

Then, comparisons are shown in Fig. 7 between σ and σ_{bt}, with Spearman Rank correlation coefficients of 0.76 with $P_{null} < 3.6 \times 10^{-8}$ for the 39 Type-1 AGN with σ_{bt15} in Bennert et al. (2015) and of 0.71 with $P_{null} < 1.7 \times 10^{-6}$ for the 37 Type-1 AGN with σ_{bt21} reported in Bennert et al. (2021). Here, in order to find more reasonable results, similar as discussed in Greene & Ho (2005), effects of SDSS instrument resolutions can be corrected on the measured stellar velocity dispersions by

$$\sigma^2 = \sigma_{obs}^2 - \sigma_{in}^2 + \sigma_{tp}^2 \quad (7)$$

where σ_{obs} represents the measured stellar velocity dispersions, $\sigma_{in} \sim 70 {\rm km \cdot s^{-1}}$ represents the SDSS instrument resolution around 4000Å, and $\sigma_{tp} \sim 30 {\rm km \cdot s^{-1}}$ represents the instrument resolution of the applied stellar template. Under considerations of uncertainties in both coordinates, through the FITEXY code, the linear correlations can be described by

$$\begin{aligned} \log(\frac{\sigma}{\rm km \cdot s^{-1}}) &= (-0.37 \pm 0.22) + \\ &\quad (1.17 \pm 0.10) \times \log(\frac{\sigma_{bt15}}{\rm km \cdot s^{-1}}) \\ \log(\frac{\sigma}{\rm km \cdot s^{-1}}) &= (-0.08 \pm 0.19) + \\ &\quad (1.04 \pm 0.09) \times \log(\frac{\sigma_{bt21}}{\rm km \cdot s^{-1}}) \end{aligned} \quad (8)$$

for the 39 Type-1 AGN with σ_{bt15} in Bennert et al. (2015), and for the 37 Type-1 AGN with σ_{bt21} reported in Bennert et al. (2021), respectively. Moreover, the mean ratio of σ to σ_{bt15} is 1.016±0.045 for the 39 Type-1 AGN in Bennert et al. (2015), and the mean ratio of σ to σ_{bt21} is 0.999±0.052 for the 37 Type-1 AGN in Bennert et al. (2021). The uncertainties of the mean ratios are estimated through the bootstrap method with 1000 loops. The strong linear correlations provide evidence to support the reliability of the measured stellar velocity dispersions in the Type-1 AGN.

Moreover, besides the reported Type-1 AGN with spatially resolved stellar velocity dispersions in Bennert et al. (2015, 2021), there are three known large samples of SDSS Type-1 AGN with measured stellar velocity dispersions, a sample of 76 Seyfert 1 galaxies in Xiao et al. (2011), the Type-1 AGN in the SDSS reverberation mapping project in Shen et al. (2015a,b); Grier et al. (2017) (SDSSRM) and a sample of low redshift Type-1 AGN in Harris et al. (2012). However, Xiao et al. (2011) mainly focused on Type-1 AGN with lower stellar velocity dispersions, and there are only 2 Type-1 AGN which have reliable stellar velocity dispersions measured through Ca II triplets in Xiao et al. (2011) and also have reliable stellar velocity dispersions measured through absorption features around 4000Å in the manuscript: SDSS J112526+022039 (plate-mjd-fiberid=0511-52636-0031) and SDSS J170246+602818 (plate-mjd-fiberid=0351-51695-0212). And there are 17 SDSSRM AGN with redshift smaller than 0.3 and with reported stellar velocity dispersions, however, none of the 17 SDSSRM AGN is included in our sample of Type-1 AGN in SDSS DR12 with reliable stellar velocity dispersions measured absorption features around 4000Å. Among the Type-1 AGN in Harris et al. (2012), there are only 5 Type-1 AGN with stellar velocity dispersions reported in Harris et al. (2012) but not reported in Bennert et al. (2015, 2021), and also included in our main sample of Type-1 AGN with measured stellar velocity dispersions through absorption features around 4000Å. Therefore, besides the 41 Type-1 AGN collected from

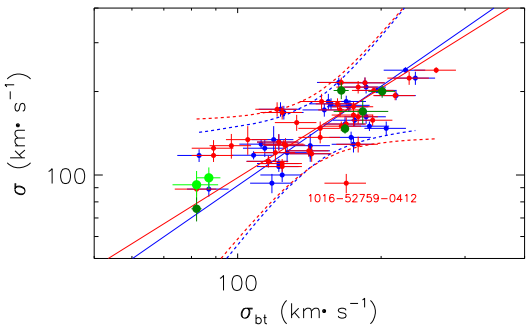

Figure 7. Correlations between the measured stellar velocity dispersions σ after corrections of instrument resolutions and the reported σ_{bt15} (in blue color) of the 39 Type-1 AGN in Bennert et al. (2015), between σ and σ_{bt21} (in red color) of the 37 Type-1 AGN in Bennert et al. (2021), and the reported σ_{xb11} (in green color) of the 2 Type-1 AGN in Xiao et al. (2011) and the reported σ_{hb12} (in dark green color) of the 5 Type-1 AGN in Harris et al. (2012). Solid blue line and dashed blue lines show the best fitting results to the correlation between σ_{bt15} and the measured σ in the manuscript after corrections of instrument resolutions, and the corresponding 99.9% confidence bands. Solid red line and dashed red lines show the best fitting results to the correlation between σ_{bt21} and the measured σ in the manuscript after corrections of instrument resolutions, and the corresponding 99.9% confidence bands.

Bennert et al. (2015, 2021), two additional Type-1 AGN are collected from Xiao et al. (2011) and 5 additional Type-1 AGN are collected from Harris et al. (2012), of which the best fitting results to absorption features around 4000Å are shown in the last 7 panels of Fig. 6 and the corresponding properties of stellar velocity dispersions are shown as solid green circles and as solid dark green circles in Fig. 7.

Moreover, as shown in Fig. 6 and Fig. 7, there are quite different stellar velocity dispersions in individual Type-1 AGN, such as in SDSS 1016-52759-0412 (SDSS J114545+554759) with stellar velocity dispersion $118 km/s$ in Bennert et al. (2015) but with $169 km/s$ in Bennert et al. (2021). Quite different stellar velocity dispersions in individual objects are mainly due to different definitions of measuring stellar velocity dispersions. The most expected result is that stellar velocity dispersions measured by different definitions lead to totally similar $M_{\rm BH} - \sigma$ measurements, therefore, stellar velocity dispersions both in Bennert et al. (2015) and in Bennert et al. (2021) are collected and compared in the manuscript. And, the mean ratios of σ to σ_{bt} well near to 1 strongly indicate that the measured stellar velocity dispersions can not lead to statistically larger or smaller stellar velocity dispersions in the Type-1 AGN by the method in the manuscript.

Second, it is interesting to compare the measured σ through absorption features around 4000Å and dispersions $\sigma_{\rm CaII}$ measured through absorption features of Ca II triplets. Among the Type-1 AGN with measured σ through absorption features around 4000Å, there are 72 AGN with high quality Ca II triplets leading to well measured reliable stellar velocity dispersions $\sigma_{\rm CaII}$ (at least 5 times larger than their corresponding uncertainties and corresponding χ^2 smaller than 2) in the SDSS spectra with median signal-to-noises larger than 20, through the same procedure applied to measure stellar velocity dispersions σ through absorption features around 4000Å. Fig. 8 shows the best fitting results to Ca II triplets of the 72 Type-1 AGN. The measured $\sigma_{\rm CaII}$ and σ are marked in each panel, and the measured $\sigma_{\rm CaII}$ are not listed in a table any more. Fig. 9 shows the comparisons between $\sigma_{\rm CaII}$ and σ, through different absorption features, with Spearman Rank correlation coefficient of 0.63 with $P_{null} \sim 4.5\times10^{-9}$. Under considerations of uncertainties in both coordinates, through the FITEXY code, the correlation can be described by

$$\log(\frac{\sigma_{\rm CaII}}{\rm km\cdot\ s^{-1}}) = (0.41\pm0.11) + (0.82\pm0.05)\times\log(\frac{\sigma}{\rm km\cdot\ s^{-1}}) \quad (9)$$

. And the mean ratio of σ to σ_{CaII} is about 0.95±0.04, with the uncertainty calculated by the bootstrap method with 1000 loops. Therefore, based on the results in Fig. 7 and in Fig. 9, the measured σ are reliable for the Type-1 AGN.

The third comparisons between stellar velocity dispersion and narrow line width are applied as indirect evidence to support reliability of the measured stellar velocity dispersions in the manuscript. Nelson & Whittle (1996) have reported a moderately strong correlation between stellar velocity dispersion and [O III] profile width, strongly indicating gravitational motion playing an important role in NLRs (narrow emission line regions) velocity field, through a large sample of Seyfert galaxies. Nelson (2000) has shown a strong correlation between BH mass and [O III] line width, indicating [O III] line width can well treated as substitute of stellar velocity dispersion. Greene & Ho (2005) have shown that line width of core components of [O III] doublets can trace stellar velocity dispersions, through a large and homogeneous sample of SDSS narrow line AGN. Komossa & Xu (2007) have shown that the [O III] line width is a good surrogate for stellar velocity dispersions, especially after removal of asymmetric blue wings and after excluding [O III] lines with strong blue-shifts. More recently, Woo et al. (2016) have reported a broad correlation between [O III] line width and stellar velocity dispersion in a large sample of Type-2 AGN, re-confirming that bulge gravitational potential plays a main role in NLRs kinematics. Bennert et al. (2018) have shown average ratio of core [O III] line width to stellar velocity dispersion is about 1, but with individual data points off by up to a factor of two, through a sample of about 80 SDSS Seyfert 1 galaxies. Therefore, comparisons between our measured stellar velocity dispersion σ and core [O III] line width σ_{O3} are applied, and shown in top left panel of Fig. 10. The mean ratios of $\log(\sigma/\sigma_{O3})$ are about 0.035±0.005 and -0.014±0.003 for the Type-1 AGN

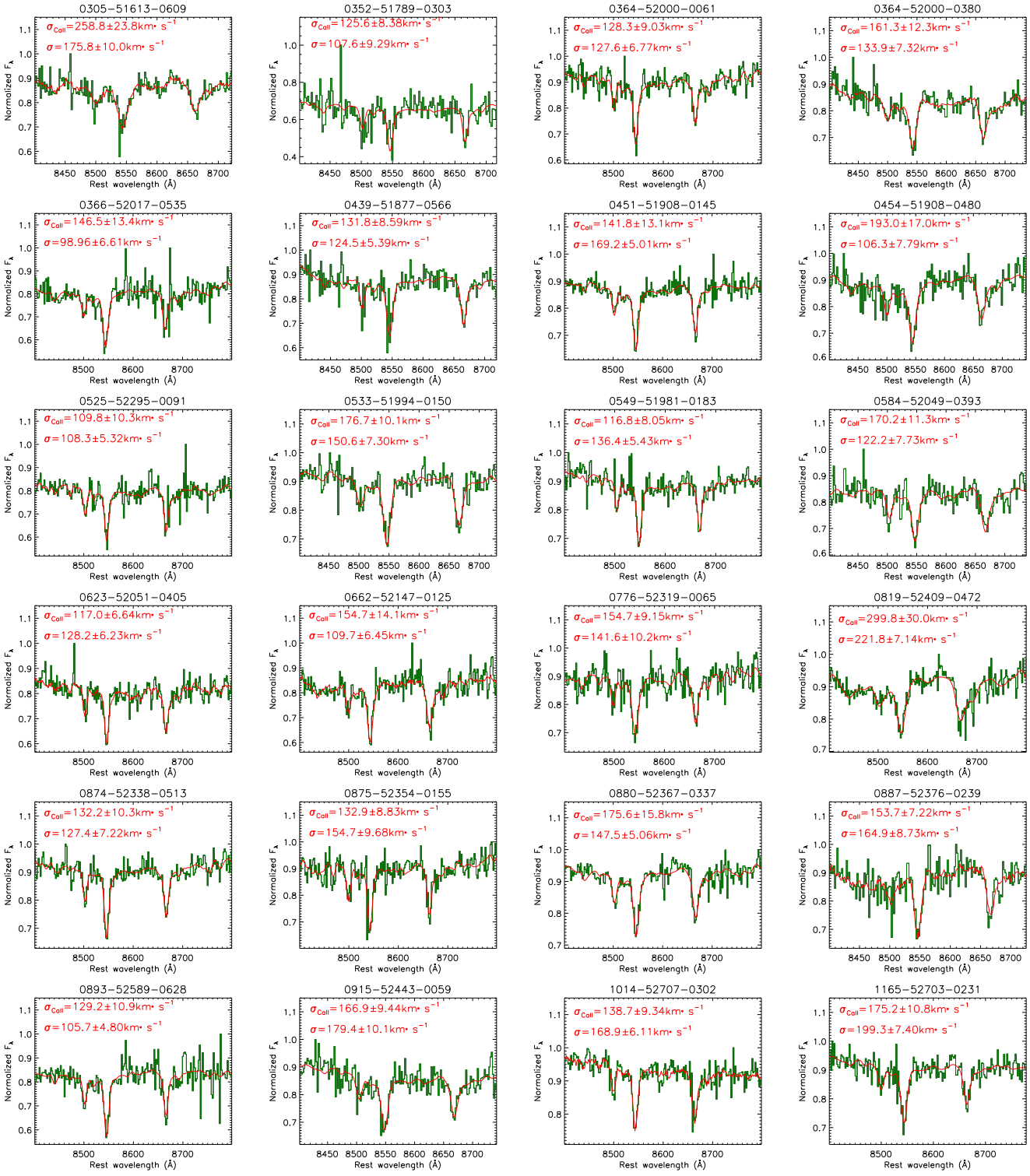

Figure 8. Best fitting results (solid red line) to Ca II triplets (solid dark green line) of the 72 Type-1 AGN. The measured stellar velocity dispersion $\sigma_{\rm CaII}$ through Ca II triplets and σ through absorption features around 4000Å are marked in red characters in each panel.

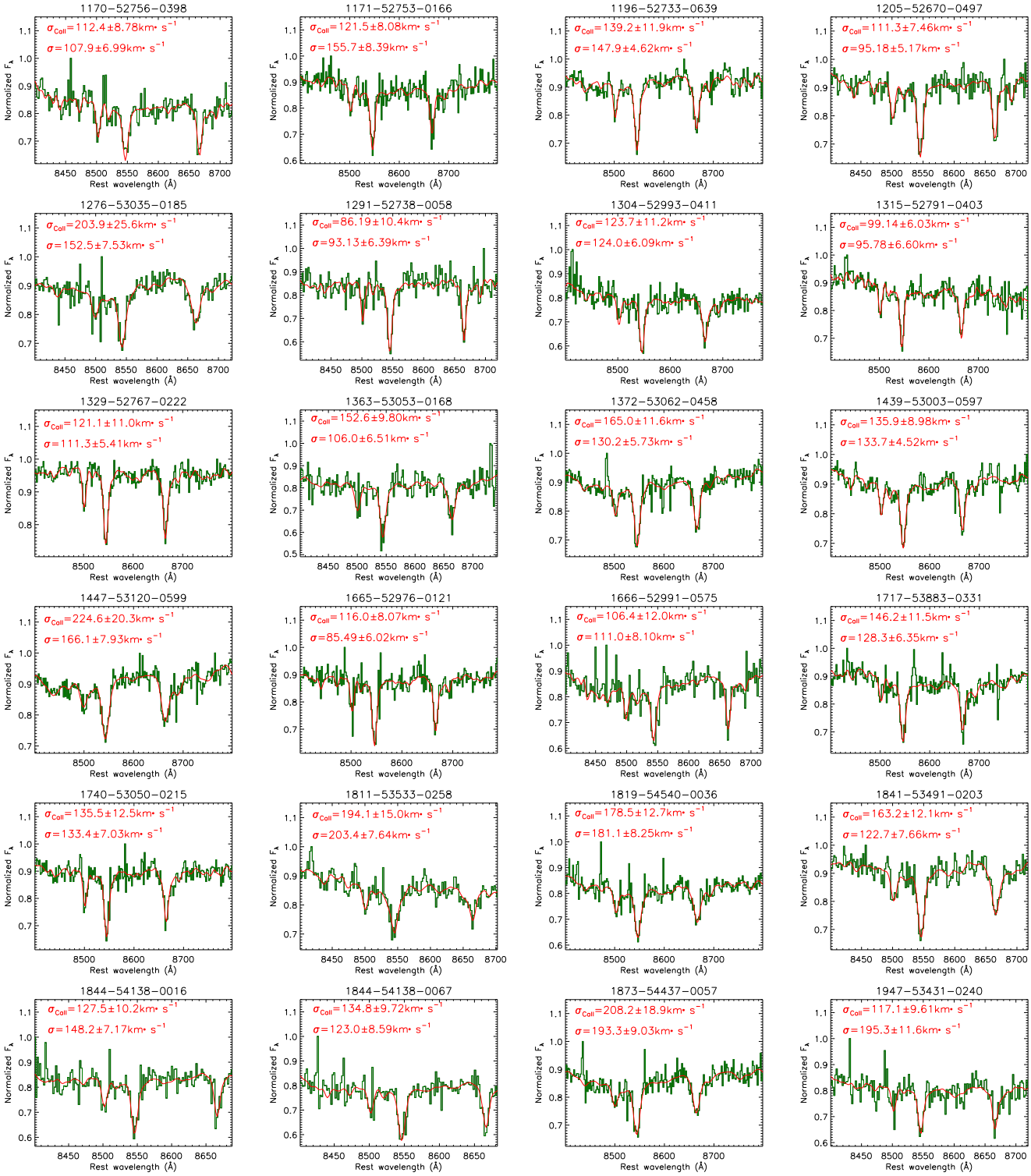

Figure 8. –to be continued

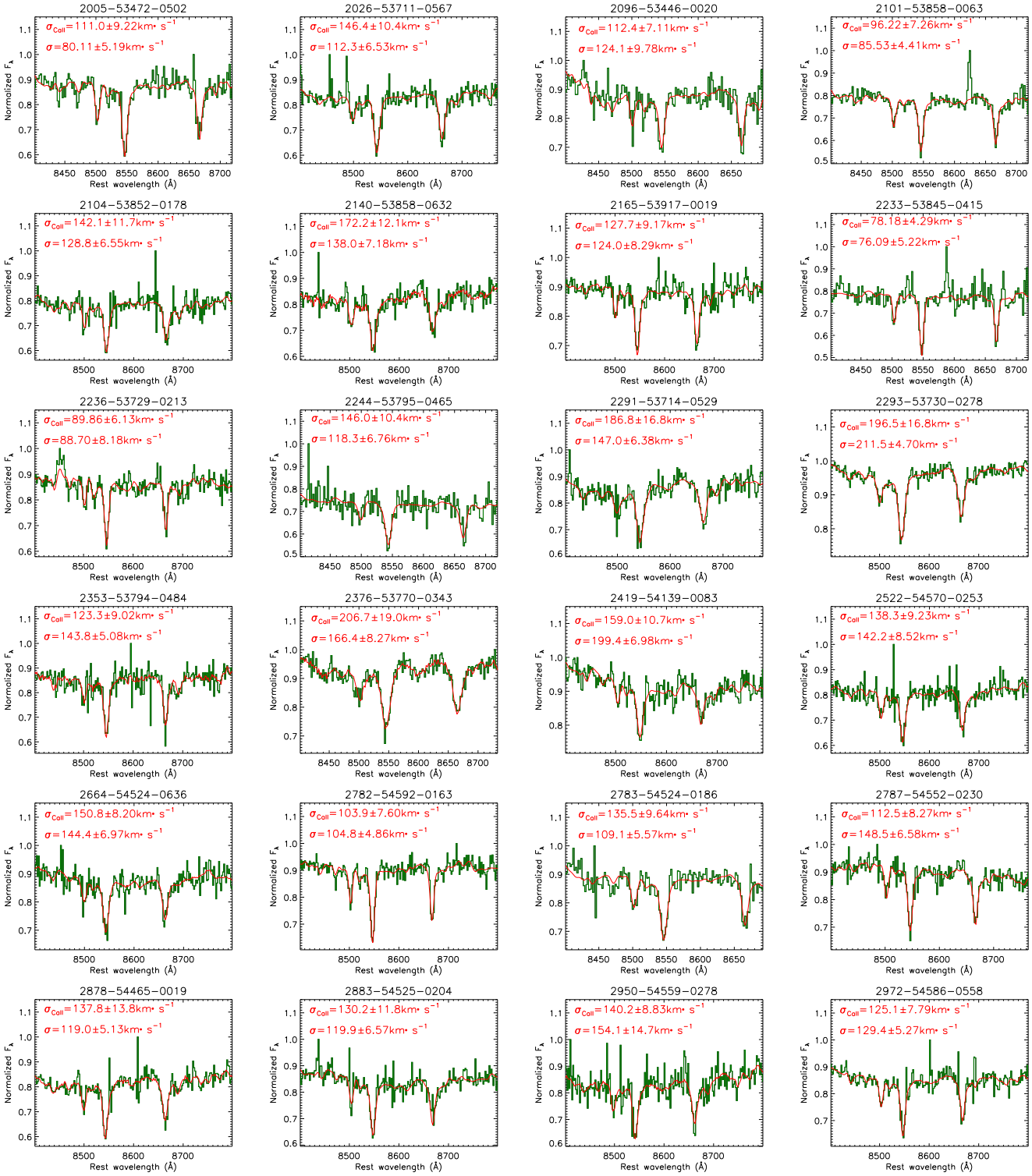

Figure 8. –to be continued

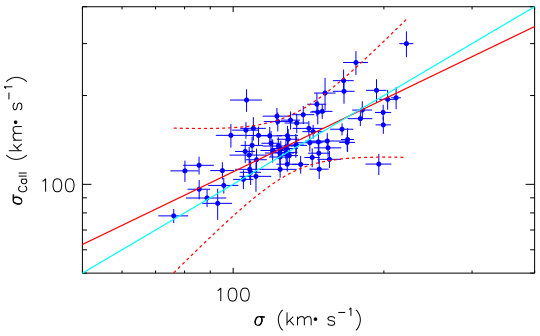

Figure 9. Correlation between σ and $\sigma_{\rm CaII}$ for the 72 Type-1 AGN with high quality Ca II triplets. Solid red line and dashed red lines show the best fitting results and the corresponding 99.99% confidence bands, and solid blue line shows $\sigma = \sigma_{\rm CaII}$.

and the Type-2 AGN respectively, with uncertainties simply estimated by the bootstrap method with 1000 loops. The average ratios $\log(\sigma/\sigma_{O3}) \sim 0$ are well consistent with reported results in the literature, to provide further clues to support the reliability of the measured stellar velocity dispersions in both the Type-2 AGN and the Type-1 AGN in the manuscript.

Besides the similar mean ratios of $\sigma/\sigma_{O3} \sim 1$ between Type-1 AGN and Type-2 AGN shown in top left panel of Fig. 10, there are different distributions of σ/σ_{O3} between Type-1 AGN and Type-2 AGN, especially the right hand side of the distributions. It is necessary and interesting to discuss whether over-estimated stellar velocity dispersions in Type-1 AGN can be applied to explain the different distributions. As is well known, there are few contaminations of stellar absorption features or continuum emissions or optical broad Fe II emissions on measured line width σ_{O3} of core components of [O III] emission lines both in Type-1 AGN as shown in Shen et al. (2011) and in Type-2 AGN as shown in Greene & Ho (2005). Top right panel of Fig. 10 shows σ_{O3} distributions of Type-1 AGN and Type-2 AGN. There are higher σ_{O3} in Type-1 AGN with mean $\log(\sigma_{O3}/{\rm km\cdot\ s^{-1}})$ about 2.179±0.005 (about 151 ± 2km$\cdot$ s^{-1}) than in Type-2 AGN with mean $\log(\sigma_{O3}/{\rm km\cdot\ s^{-1}})$ about 2.127±0.004 (about 133 ± 2km$\cdot$ s^{-1}). Besides the different σ_{O3} distributions shown in top right panel of Fig. 10 for the samples of Type-1 AGN and Type-2 AGN with quite different distributions of σ/σ_{O3}, two subsamples[4] of 5468 Type-1 AGN and 5468 Type-2 AGN are collected to have the same distributions of σ/σ_{O3} which is shown in bottom left panel of Fig. 10 with significance levels higher than 99.99% through the two-sided Kolmogorov-Smirnov statistic technique. If there were over-estimated stellar velocity dispersions in Type-1 AGN leading to the different distributions shown in top left panel of Fig. 10, there should be quite smaller σ_{O3} difference between Type-1 AGN and Type-2 AGN in the subsamples than in the main samples. However, as shown distributions in bottom right panel of Fig. 10 of σ_{O3} in the Type-1 AGN and Type-2 AGN in the subsamples which have the same distributions of σ/σ_{O3}, the mean values $\log(\sigma_{O3}/{\rm km\cdot\ s^{-1}})$ are about 2.182±0.005 and 2.119±0.004 in the Type-1 AGN and in the Type-2 AGN in the subsamples, respectively. The quite similar mean values of σ_{O3} between Type-1 AGN and Type-2 AGN in the subsamples and in the main samples strongly indicate that the different distributions of σ/σ_{O3} shown in top left panel of Fig. 10 are not due to over-estimated stellar velocity dispersions in Type-1 AGN, but mainly due to different distributions of σ_{O3} between Type-1 AGN and Type-2 AGN. Therefore, results in Fig. 10 can be accepted as indirect evidence to support the reliability of our measured stellar velocity dispersions, but there are no further discussions on the different distributions of σ_{O3} in Type-1 AGN and Type-2 AGN which is beyond the scope of the manuscript and have few effects on our final conclusions in the manuscript.

[4] It is quite easy to create the two subsamples, based on the shown distributions of σ/σ_{O3} in top left panel of Fig. 10. Here, there are no detailed descriptions on how to create the subsamples, but quite similar as what will be done in Section 5.3.

5. MAIN RESULTS AND DISCUSSIONS

5.1. *Direct comparisons of stellar velocity dispersions*

Based on the measured σ through absorption features around 4000Å, left panel of Fig. 11 shows the direct σ comparisons between the largest sample of 6260 Type-1 AGN and the largest sample of 15353 Type-2 AGN in SDSS DR12. The mean $\log(\sigma)$ are about $\log(\sigma/{\rm km\cdot\ s^{-1}}) \sim 2.199 \pm 0.006$ ($\sigma \sim 158\pm3{\rm km\cdot\ s^{-1}}$) and $\log(\sigma/{\rm km\cdot\ s^{-1}}) \sim 2.117\pm0.004$ ($\sigma \sim 132 \pm 2{\rm km\cdot\ s^{-1}}$) for the Type-1 AGN and the Type-2 AGN, respectively, indicating statistically larger stellar velocity dispersions in Type-1 AGN. Uncertainty of each mean value is determined by the bootstrap method with 1000 loops. Meanwhile, in order to ensure few effects of data quality on the different distributions of $\log(\sigma)$, there are 1680 Type-1 AGN and 8535 Type-2 AGN collected through the criterion that the measured stellar velocity dispersions at least 10 times larger than their uncertainties. The corresponding comparison results on the high quality stellar velocity dispersions are shown in right panel of Fig. 11, with mean $\log(\sigma)$ about $\log(\sigma/{\rm km\cdot\ s^{-1}}) \sim 2.222 \pm 0.003$ ($\sigma \sim 167 \pm 3{\rm km\cdot\ s^{-1}}$) and $\log(\sigma/{\rm km\cdot\ s^{-1}}) \sim 2.144\pm0.002$ ($\sigma \sim 138\pm1{\rm km\cdot\ s^{-1}}$) for the Type-1 AGN and the Type-2 AGN, respectively, with uncertainty of each mean value determined by the bootstrap method with 1000 loops.

Moreover, considering the discussed results in Section 3 that the measured stellar velocity dispersions in Type-1 AGN are about 4% larger than the intrinsic values, the corrected mean σ are about $\sigma \sim 152 \pm 2{\rm km\cdot\ s^{-1}}$ and $\sigma \sim 161 \pm 2{\rm km\cdot\ s^{-1}}$ for the 6260 Type-1 AGN and for

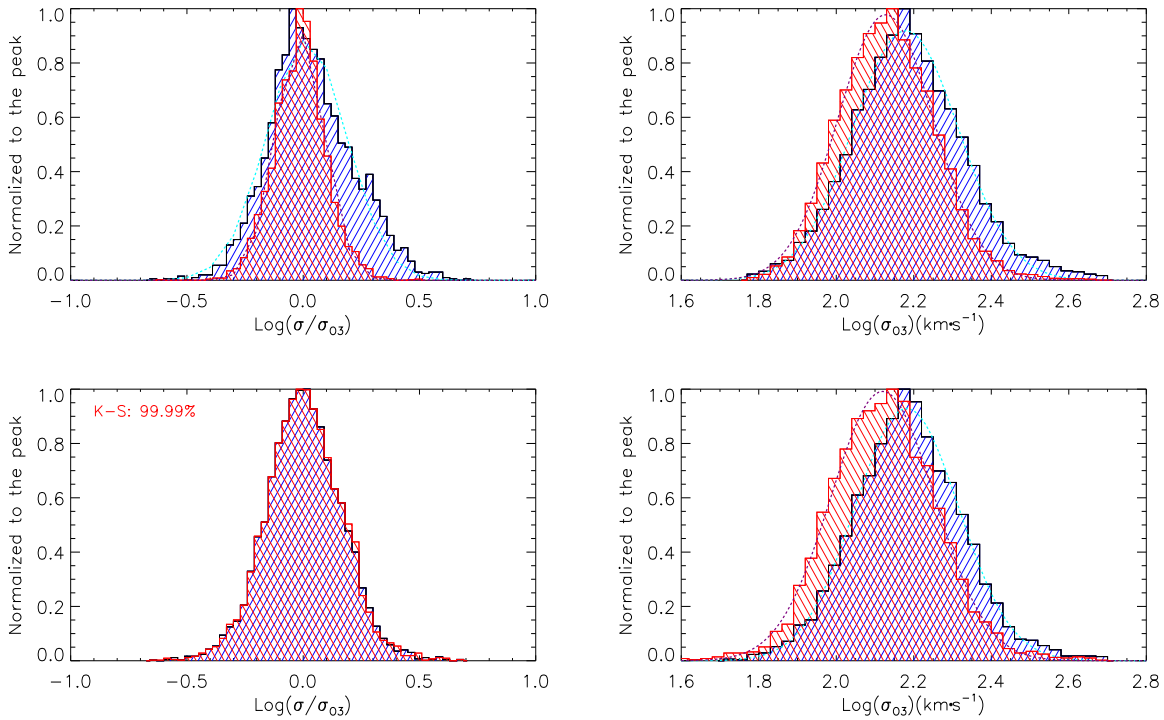

Figure 10. Top left panel shows distributions of σ/σ_{O3} of our measured stellar velocity dispersions σ to the core [O III] line width σ_{O3} in the 6260 Type-1 AGN and in the 15353 Type-2 AGN in the main samples. Top right panel shows distributions of σ_{O3} in the 6260 Type-1 AGN and in the 15353 Type-2 AGN in the main samples. Bottom left panel shows distributions of σ/σ_{O3} in the 5468 Type-1 AGN and in the 5468 Type-2 AGN in the subsamples which have the same distributions of σ/σ_{O3}. Bottom right panel shows distributions of σ_{O3} in the 5468 Type-1 AGN and in the 5468 Type-2 AGN in the subsamples which have the same distributions of σ/σ_{O3}. In each panel, histogram filled by blue lines and by red lines show distributions of the Type-1 AGN and the Type-2 AGN, respectively, dashed line in purple and in cyan represent the corresponding best fitting Gaussian profiles for the distributions of the Type-2 AGN and of the Type-1 AGN, respectively. In bottom left panel, the Kolmogorov-Smirnov statistic technique provided significance level is marked in red characters.

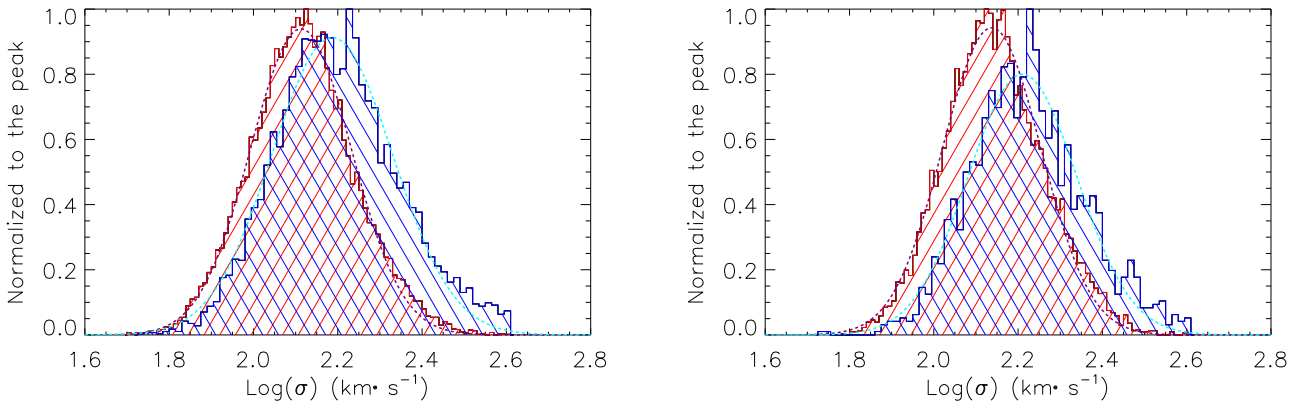

Figure 11. Left panel shows distributions of stellar velocity dispersions of the 6260 Type-1 AGN (histogram filled by blue lines) and the 15353 Type-2 AGN (histogram filled by red lines), respectively. Right panel shows distributions of high quality stellar velocity dispersions (10 times larger than their uncertainties) of the 1680 Type-1 AGN (histogram filled by blue lines) and the 8535 Type-2 AGN (histogram filled by red lines), respectively. In each panel, dashed lines in purple and in cyan represent the corresponding best fitting Gaussian profiles for the $\log(\sigma)$ distributions of the Type-2 AGN and of the Type-1 AGN, respectively.

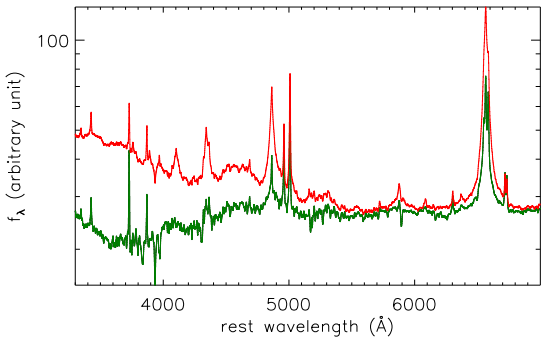

Figure 12. The inverse variance weighted mean spectra of Type-1 AGN (solid dark green line) with stellar velocity dispersions well measured through absorption features around 4000Å and of the other Type-1 AGN (solid red line) without apparent absorption features around 4000Å.

the 1680 Type-1 AGN with high quality stellar velocity dispersions, respectively, to re-confirm statistically larger stellar velocity dispersions in Type-1 AGN. After considering the measured stellar velocity dispersions in Type-1 AGN about 4% larger than the intrinsic values, the Students T-statistic technique is re-applied to determine the different mean values of $\log(\sigma)$ between Type-1 AGN (with measured stellar velocity dispersions scaled by 0.96) and Type-2 AGN with confidence level higher than 10sigma, and the two-sided Kolmogorov-Smirnov statistic technique indicates stellar velocity dispersions of the Type-1 AGN and the Type-2 AGN obey the same distributions of $\log(\sigma)$ with significance level smaller than 10^{-25}. Therefore, in spite of the following necessary discussed effects, the basic results can be found that Type-1 AGN have their stellar velocity dispersions statistically 16% larger than Type-2 AGN.

5.2. *Dependence of stellar velocity dispersion on [O III] luminosity*

As the shown results in section 2, there are half of Type-1 AGN of which stellar velocity dispersions σ can not be well measured. Therefore, in the subsection, necessary discussions are given on expected probable properties of the intrinsic stellar velocity dispersions of the half of Type-1 AGN without measured σ in the parent sample.

There is only one probability leading to stellar velocity dispersions not be well measured through absorption features around 4000Å in Type-1 AGN, the host galaxy contributions are weak enough that absorption features around 4000Å are overwhelmed in emission features of AGN activities. Therefore, it is interesting to check spectral features of the Type-1 AGN with and without measured σ. Fig. 12 shows the inverse variance weighted mean spectra of the 6260 Type-1 AGN with well measured σ and of the other Type-1 AGN with σ not measured due to unapparent absorption features around 4000Å. The mean spectra with bluer continuum emissions around 4000Å can be well applied to confirm that the half of Type-1 AGN without measured σ are mainly due to unapparent absorption features around 4000Å which are overwhelmed by emission features of central AGN activities.

Meanwhile, left panel Fig. 13 shows dependence of measured σ on total [O III] line luminosity L_{O3} of the 6260 Type-1 AGN with well measured σ. The dependence could provide clues to expected properties of intrinsic σ of the other half of Type-1 AGN without measured σ in the parent sample. There is a positive linear correlation between σ and L_{O3} with Spearman Rank correlation coefficient of 0.38 with $P_{null} < 10^{-10}$. And the positive linear correlation can be described by

$$\log(\frac{\sigma}{\mathrm{km}\cdot\ \mathrm{s}^{-1}}) \sim -4.45 + 0.16\times\log(\frac{L_{O3}}{\mathrm{erg}\cdot\ \mathrm{s}^{-1}}) \quad (10)$$

indicating that Type-1 AGN with higher [O III] line luminosity will have statistically larger intrinsic σ. Then, right panel of Fig. 13 shows distributions of $\log(L_{O3}/\mathrm{erg}\cdot\ \mathrm{s}^{-1})$ with mean values of $\sim 41.245\pm0.006$ ($L_{O3}\sim(1.76\pm0.02)\times10^{41}\mathrm{erg}\cdot\ \mathrm{s}^{-1}$) and $\sim 41.340\pm0.008$ ($L_{O3}\sim(2.19\pm0.04)\times10^{41}\mathrm{erg}\cdot\ \mathrm{s}^{-1}$) of the Type-1 AGN with and without well measured σ. The uncertainties of the mean values are estimated by the bootstrap method with 1000 loops. And the two-sided Kolmogorov-Smirnov statistic technique indicates the two distributions of $\log(L_{O3})$ obey the same distributions with significance level only about 10^{-22}. Therefore, the half of Type-1 AGN without measured σ should have statistically larger σ (at least not smaller) than the 6260 Type-1 AGN with apparent absorption features around 4000Å. Therefore, considering the half of Type-1 AGN without well measured σ, the mean σ of all the 12342 Type-1 AGN in the parent sample should be larger than the ones shown in Fig. 11.

Moreover, although only dozens of Type-1 AGN have Ca II triplets in SDSS spectra, mean spectra around 8500Å of the low redshift Type-1 AGN with and without measured σ are well checked, in order to examine whether the Type-1 AGN without measured σ through absorption features around 4000Å have statistically larger σ, based on the σ measured through Ca II triplets. Fig. 14 shows the mean spectra around 8500Å of Type-1 AGN with and without measured σ through absorption features around 4000Å, and the best fitting results by single stellar template as what have been done to absorption features around 4000Å. The determined stellar velocity dispersions are about $\sigma_{CaII}\sim 153\mathrm{km}\cdot\ \mathrm{s}^{-1}$ and $\sigma_{CaII}\sim 142\mathrm{km\,cot\ s}^{-1}$ for the Type-1 AGN without and with apparent absorption features around 4000Å, respectively. The results are consistent with the expected larger σ of the Type-1 AGN without apparent absorption features around 4000Å. Therefore, considering the half Type-1 AGN without measured σ will lead to statistically larger σ for all the 12342 Type-1 AGN than those shown in Fig. 11 for the 6260 Type-1 AGN in the main sample.

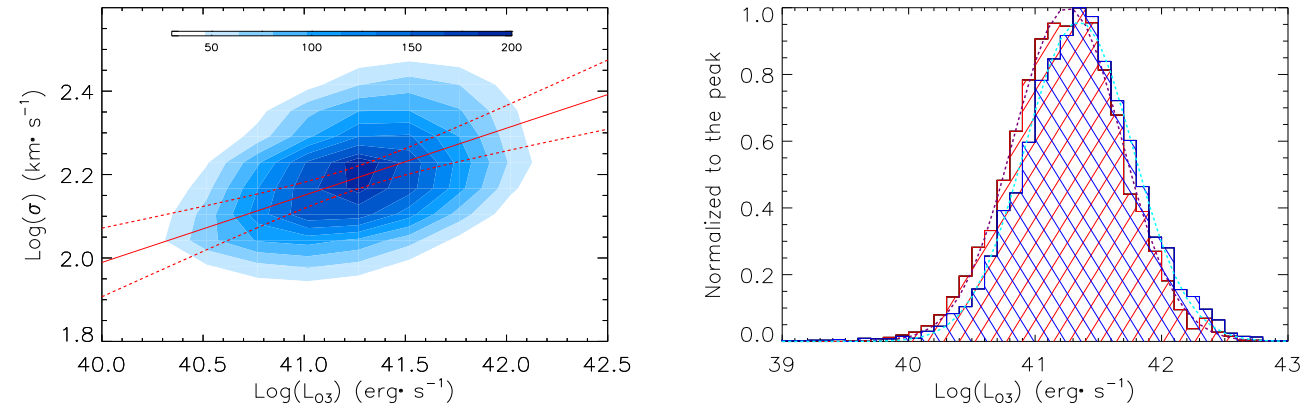

Figure 13. Left panel shows dependence of σ on total [O III] line luminosity L_{O3} of the 6260 Type-1 AGN with well measured σ. Solid red line and dashed red lines show the best-fitting results and the corresponding 5sigma confidence bands, respectively. Right panel shows L_{O3} distributions of the Type-1 AGN with (histogram filled with red lines) and without (histogram filled with blue lines) apparent absorption features around 4000Å. Dashed lines in purple and in cyan represent the corresponding best-fitting Gaussian profiles for the L_{O3} distributions of the Type-1 AGN with and without measured stellar velocity dispersions, respectively.

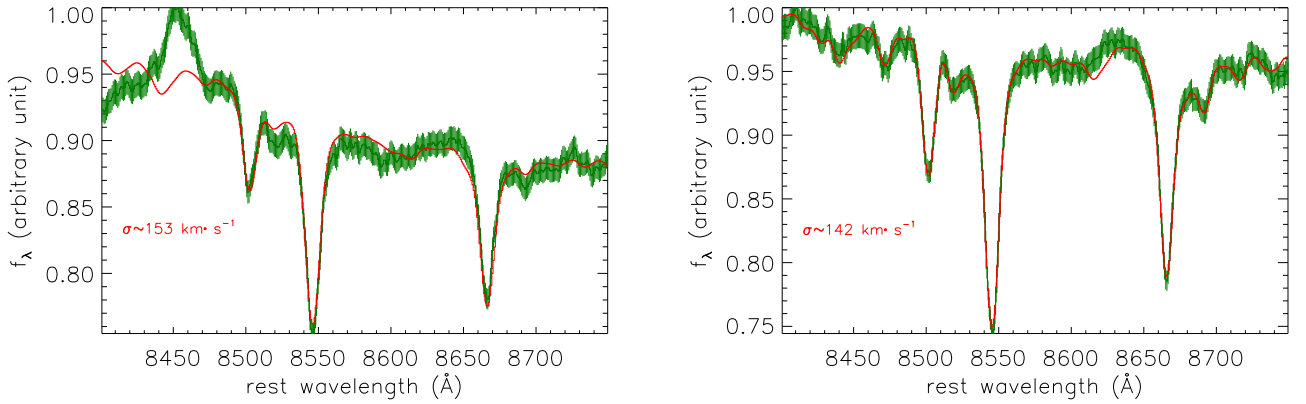

Figure 14. The mean spectra around 8500Å of the Type-1 AGN without (left panel) and with (right panel) apparent absorption features around 4000Å. Solid red line shows the best-fitting results to Ca II triplet. The measured stellar velocity dispersion through Ca II triplet is marked in red characters in each panel.

Furthermore, as discussed in Kewley et al. (2006), ratio of [O III] line luminosity to σ^4 (applied to trace central BH mass) can be accepted as a good indicator of central accretion rate relative to the Eddington ratio, leading to continuous sequence for different subclasses of Type-2 AGN. Here, properties of L_{O3}/σ^4 are checked for Type-1 AGN and Type-2 AGN, with L_{O3} in unit of erg $\cdot$ s^{-1} and σ in unit of km $\cdot$ s^{-1}.

Before proceeding further, as discussed results on extended components of [O III] doublets in AGN in Zhang et al. (2017, 2021), not line luminosity of total [O III]λ5007Å but of the core component of [O III]λ5007Å is applied to check the properties of L_{O3}/σ^4 of Type-1 AGN and Type-2 AGN, because of seriously obscured extended components of [O III]λ5007Å in Type-2 AGN and of the strong linear correlation between AGN continuum luminosity and the luminosity of the core component of [O III]λ5007Å. Properties of L_{O3}/σ^4 are shown in Fig. 15. Different L_{O3}/σ^4 can be confirmed between Type-1 AGN and Type-2 AGN. There are positive linear correlations between L_{O3}/σ^4 and σ with Spearman rank correlation coefficients of about 0.38 and 0.31 with $P_{null} < 10^{-10}$ for the Type-1 AGN and the Type-2 AGN, and the linear correlations can be described by

$$\log(\frac{\sigma}{\mathrm{km}\cdot\ \mathrm{s}^{-1}}) \sim 8.47 - 0.19\times\log(\frac{L_{O3}}{\sigma^4})\ \ (Type-1)$$
$$\log(\frac{\sigma}{\mathrm{km}\cdot\ \mathrm{s}^{-1}}) \sim 4.96 - 0.09\times\log(\frac{L_{O3}}{\sigma^4})\ \ (Type-2) \quad (11)$$

The mean $\log(L_{O3}/\sigma^4)$ are about 32.448±0.009 and 31.948±0.008 of the Type-1 AGN and the Type-2 AGN respectively, with the uncertainties estimated by the bootstrap

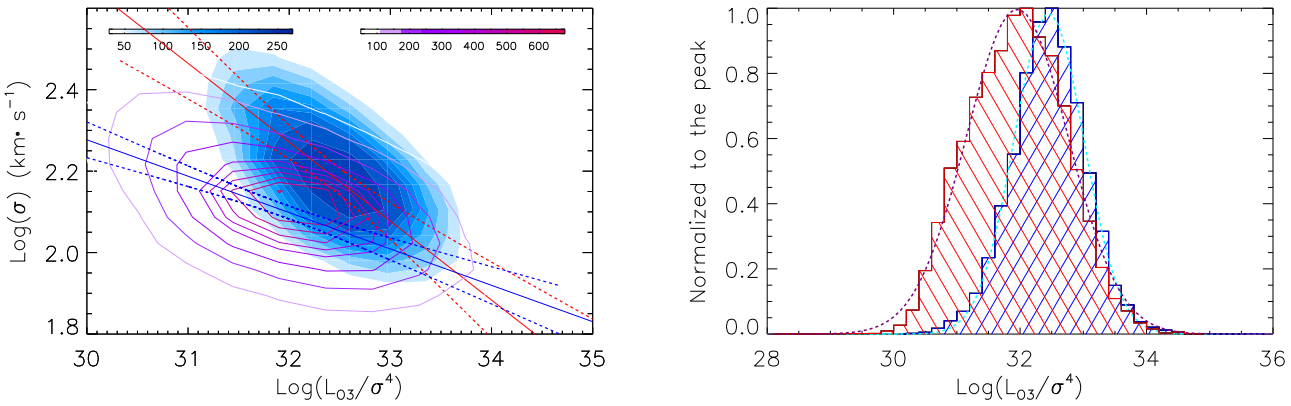

Figure 15. Left panel shows dependence of σ on L_{O3}/σ^4 for the Type-1 AGN (contour filled by bluish colors) and the Type-2 AGN (contour levels by reddish lines). Solid red line and dashed red lines are for the best-fitting results and the corresponding 5sigma confidence bands for the Type-1 AGN. Solid blue line and dashed blue lines are for the best-fitting results and the corresponding 5sigma confidence bands for the Type-2 AGN. Right panel shows L_{O3}/σ^4 distributions of the Type-1 AGN (histogram filled with blue lines) and Type-2 AGN (histogram filled with red lines).

method with 1000 loops. Therefore, Type-1 AGN and Type-2 AGN have quite different properties of $\log(L_{O3}/\sigma^4)$. Actually, line luminosity of total [O III]λ5007Å can lead to the similar results on the quite different ratios of total [O III] line luminosity to σ^4 in Type-1 AGN and Type-2 AGN. Different $\log(L_{O3}/\sigma^4)$ provide different central activity properties of the collected Type-1 AGN and Type-2 AGN, indicating further effects should be carefully considered on the shown results in Fig. 11.

5.3. *Necessary effects on the comparisons of stellar velocity dispersions*

Effects of different redshift are firstly considered on the results shown in Fig. 11, because different redshift provides different evolutionary histories of host galaxies and central BHs. Different distributions of redshift of Type-1 AGN and Type-2 AGN are shown in top left panel of Fig. 16. Mean redshifts are about 0.162±0.001 and 0.104±0.001 of the Type-1 AGN and the Type-2 AGN, respectively. Meanwhile, effects of different central AGN activities should be considered, because BH mass is one of fundamental parameters relative to AGN activities. Here, the narrow emission line flux rations of core component of [O III]λ5007Å to narrow Hβ (O3HB) and of [N II]λ6583Å to narrow Hα (N2HA) are mainly considered to trace central AGN activities, the commonly applied ratios in the well-known Baldwin-Phillips-Terlevich diagrams (Baldwin et al. 1981; Kewley et al. 2001; Kauffmann et al. 2003a; Kewley et al. 2006, 2019; Zhang et al. 2020). Different distributions of O3HB and N2HA are shown in left middle two panels of Fig. 16 with mean values of $\log(O3HB)$ ($\log(N2HA)$) about 0.754±0.008 and 0.454±0.003 (-0.091±0.004 and -0.057±0.002) of the Type-1 AGN and the Type-2 AGN, respectively. Moreover, considering emission luminosity also sensitively depending on central AGN activities, effects of different [O III] line luminosity L_{O3} of core component are also well checked. Different distributions of L_{O3} are shown in the bottom left panel of Fig. 16, with mean values of $\log(L_{O3}/(\mathrm{erg/s}))$ about 40.945±0.008 and 40.282±0.007 of the Type-1 AGN and the Type-2 AGN, respectively. Uncertainty of each mean value of each distribution in the left panels of Fig. 16 is simply estimated by the bootstrap method with 1000 loops.

Before proceeding further, besides the distributions of O3HB and N2HA in left panels of Fig. 16, it is interesting to show properties of the collected Type-1 AGN and Type-2 AGN in the well-known BPT diagram in left panel of Fig. 17, to show different locations between Type-1 AGN and Type-2 AGN in the BPT diagram. There are quite different central positions (marked as thick pluses) for the Type-1 AGN and the Type-2 AGN in the BPT diagram, to provide further clues to discuss effects of different central AGN activities on our final results on the different stellar velocity dispersions between Type-1 AGN and Type-2 AGN. Meanwhile, through the strip marked by dashed cyan lines with width about 0.1 in the BPT diagram in left panel of Fig. 17, the 1044 Type-1 AGN and the 4202 Type-2 AGN lying in the strip are collected to simply check effects of AGN activities on stellar velocity dispersions comparisons. The stellar velocity dispersion comparisons are shown in right panel of Fig. 17 of the 1044 Type-1 AGN and the 4202 Type-2 AGN in the strip, with mean $\log(\sigma)$ about $\log(\sigma/\mathrm{km\cdot\ s^{-1}}) \sim 2.196 \pm 0.005$ ($\sigma \sim 157 \pm 2\mathrm{km\cdot\ s^{-1}}$) and $\log(\sigma/\mathrm{km\cdot\ s^{-1}}) \sim 2.101 \pm 0.002$ ($\sigma \sim 126 \pm 1\mathrm{km\cdot\ s^{-1}}$) for the 1044 Type-1 AGN and the 4202 Type-2 AGN in the strip, respectively. The uncertainties of the mean values are determined by the bootstrap method with 1000 loops. Con-

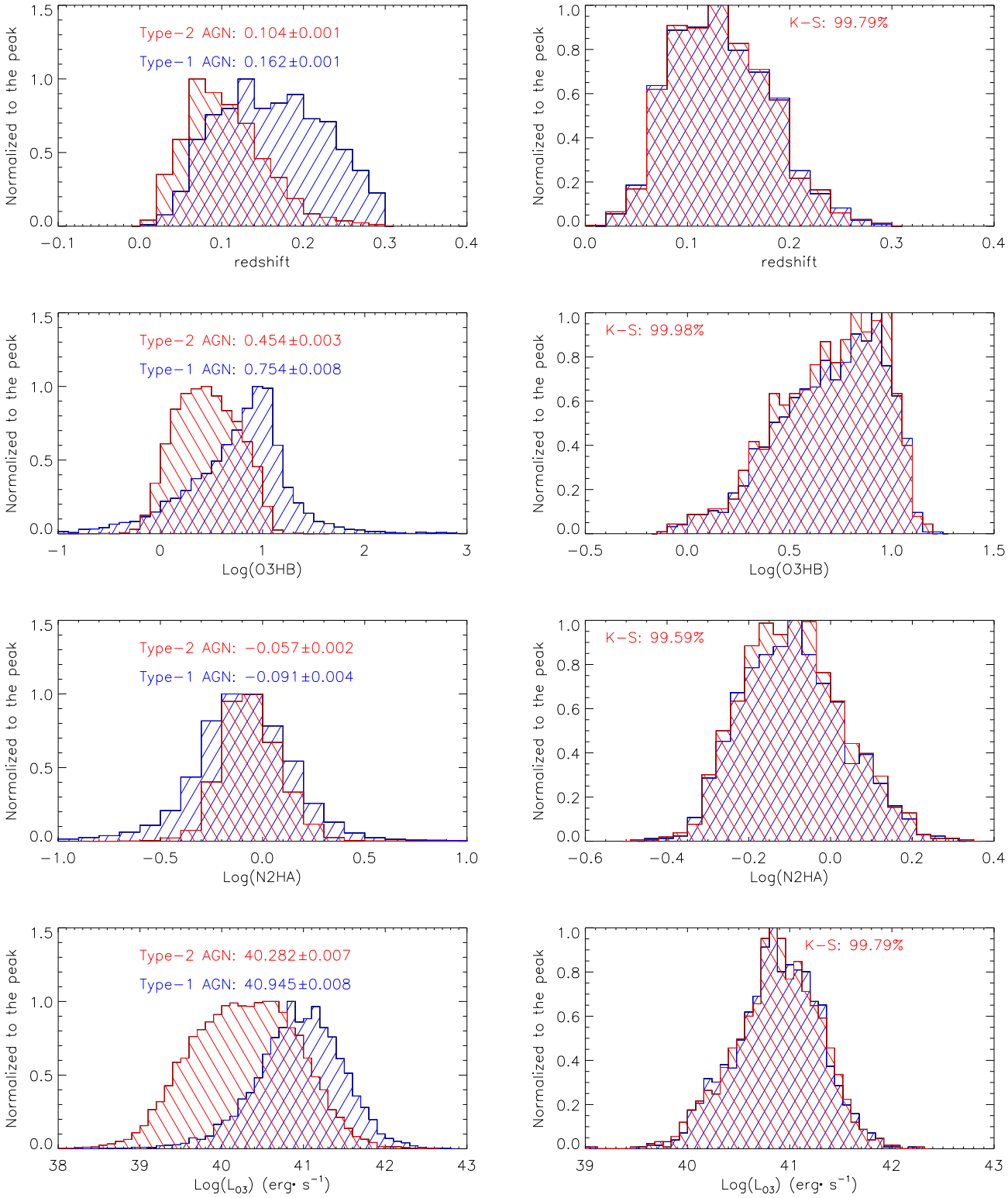

Figure 16. Distributions of redshift (top panels), of narrow line flux ratios of O3HB and N2HA (middle two panels) and of luminosity of core components of [O III] line (bottom panels) of the Type-1 AGN (histogram filled with blue lines) and Type-2 AGN (histogram filled with red lines) in the main samples (left panels) and in the subsamples (right panels). In each right panel, the Kolmogorov-Smirnov statistic technique provided significance level is marked in red characters. In each left panel, the mean values of the Type-1 AGN and the Type-2 AGN are marked in blue and red characters in top region.

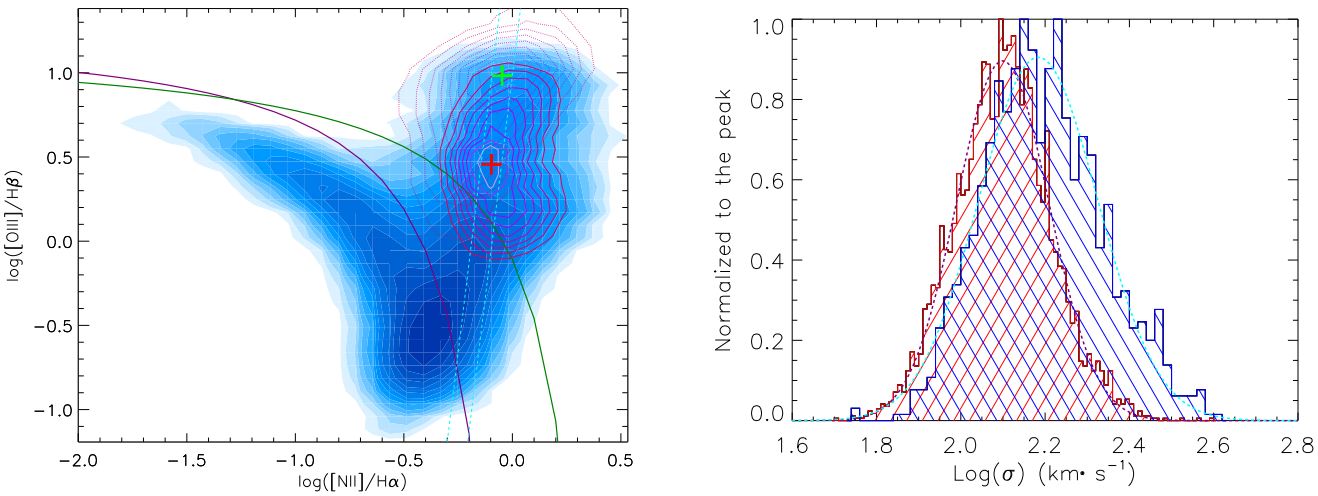

Figure 17. Left panel shows type-1 AGN and Type-2 AGN in the BPT diagram of O3HB versus N2HA. Contour filled with bluish colors represents the results for all the narrow emission line galaxies collected from SDSS DR12. Contour with levels as solid reddish lines and with levels as dotted reddish lines represent the results for the Type-2 AGN and the Type-1 AGN with reliable stellar velocity dispersions in the manuscript, respectively. Thick pluses in red and in green mark the central positions of the contours for the Type-2 AGN and for the Type-1 AGN, respectively. Solid purple line and solid dark green line show the dividing lines between different kinds of narrow emission line galaxies in Kewley et al. (2006); Kauffmann et al. (2003a). Dashed cyan lines mark the strip applied to collect Type-1 AGN and Type-2 AGN to simply check effects of AGN activities on stellar velocity dispersion comparisons. Right panel shows the results Similar as Fig. 11, but for the 1044 Type-1 AGN and the 4202 Type-2 AGN covered in the strip shown in left panel. The symbols and line styles have the same meanings as those in Fig. 11.

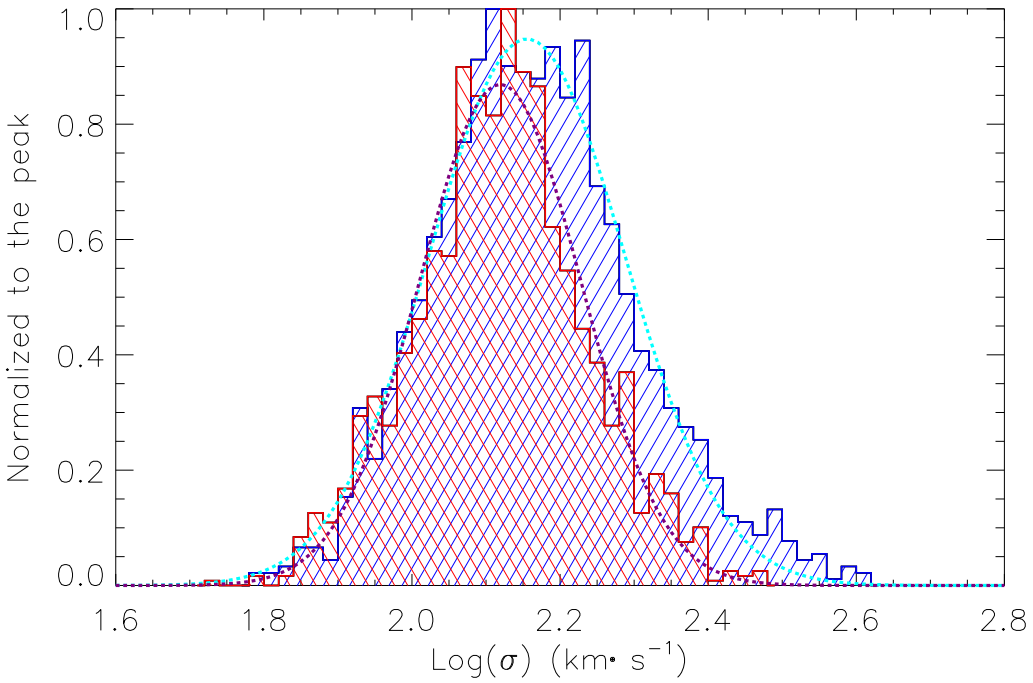

Figure 18. Similar as Fig. 11, but for the 1445 Type-1 AGN and the 1445 Type-2 AGN in the subsamples, which have the same distributions of z, O3HB, N2HA and L_{O3}. The symbols and line styles have the same meanings as those in Fig. 11.

sidering the measured stellar velocity dispersions in Type-1 AGN 4% higher than the intrinsic values, the corrected mean stellar velocity dispersion is about $\sigma \sim 151 \pm 2\mathrm{km}\cdot \mathrm{s}^{-1}$ in the 1044 Type-1 AGN, still indicating higher stellar velocity dispersions in Type-1 AGN. Different strips in the BPT diagram can lead to the similar higher stellar velocity dispersions in Type-1 AGN covered in the strips. Here, we do not show more results in different strips, however, the results indicate more detailed discussions are necessary on effects of AGN activities.

In order to ignore the necessary effects of different distributions of redshift (z), narrow line flux ratios (O3HB and N2HA) and line luminosity of core components of [O III] line (L_{O3}) on direct σ comparisons, the most convenient way is to create two subsamples of Type-1 AGN and Type-2 AGN having the same distributions of z, O3HB, N2HA and L_{O3}. Based on the measured z, O3HB, N2HA and L_{O3} of the 6260 Type-1 AGN and the 15353 Type-2 AGN in the main samples, it is easy to create a subsample of Type-2 AGN having the same distributions of z, O3HB, N2HA and L_{O3} as those of the Type-1 AGN in the subsample, through finding minimum parameter distance $D_p < D_{cri}$ calculated as

$$\begin{aligned} D_{p,\,i} &= D_{z,\,i} + D_{O3HB,\,i} + D_{N2HA,\,i} + D_{L_{O3},\,i} \\ &= (\frac{z_{1,i} - z_2}{sca_z})^2 + (\frac{O3HB_{1,i} - O3HB_2}{sca_{O3HB}})^2 \\ &\quad + (\frac{N2HA_{1,i} - N2HA_2}{sca_{N2HA}})^2 \\ &\quad + (\frac{L_{O3,\,1,\,i} - L_{O3,\,2}}{sca_{L_{O3}}})^2 \quad for\ i = 1, \ldots, N_1 \end{aligned} \tag{12}$$

where $z_{1,\,i}$, $O3HB_{1,\,i}$, $N2HA_{1,\,i}$ and $L_{O3,\,1,\,i}$ mean parameters of the ith Type-1 AGN in the main sample ($N_1 = 6260$), z_2, $O3HB_2$, $N2HA_2$ and $L_{O3,\,2}$ mean parameters of all $N_2 = 15353$ ($N_2 > N_1$) Type-2 AGN in the main sample, sca_z, sca_{O3HB}, sca_{N2HA} and $sca_{L_{O3}}$ are scale factors leading to D_z, D_{O3HB}, D_{N2HA} and $D_{L_{O3}}$ not much different in quantity, and D_{cri} means a critical value to prevent high D_p leading to much different distributions of z, O3HB, N2HA and L_{O3} between the created final two subsamples. Then, based on $sca_z \sim 0.0015$ and $sca_{O3HB} \sim 0.006$, $sca_{N2HA} \sim 0.0035$ and $sca_{L_{O3}} \sim 0.02$ and $D_{cri} \sim 80$, one subsample of 1445 Type-1 AGN and one subsample of 1445 Type-2 AGN are created, which have the same distributions of z, O3HB, N2HA and L_{O3} with significance levels higher than 99.5% through the two-sided Kolmogorov-Smirnov statistic technique. Certainly, each object in the main samples is selected once in the two subsamples. The distributions of z, O3HB, N2HA and L_{O3} for the AGN in the subsamples are shown in right panels of Fig. 16. The parameters, such as σ, z, O3HB, N2HA and L_{O3}, etc., of the 1445 Type-1 AGN and the 1445 Type-2 AGN in the subsamples are listed in Table 1 and in Table 2.

Similar as Fig. 11 but for the 1445 Type-1 AGN and the 1445 Type-2 AGN in the subsamples, stellar velocity dispersion comparisons are shown in Fig. 18. After considering necessary effects, statistically larger σ can also be clearly confirmed in Type-1 AGN with mean $\log(\sigma/\mathrm{km}\cdot \mathrm{s}^{-1}) \sim 2.166 \pm 0.005$ ($\sigma \sim 147 \pm 2\mathrm{km}\cdot \mathrm{s}^{-1}$) than in Type-2 AGN with mean $\log(\sigma/\mathrm{km}\cdot \mathrm{s}^{-1}) \sim 2.115 \pm 0.004$ ($\sigma \sim 130 \pm 2\mathrm{km}\cdot \mathrm{s}^{-1}$). Considering the measured stellar velocity dispersions in Type-1 AGN 4% higher than the intrinsic values, the corrected mean stellar velocity dispersions is about $\sigma \sim 142 \pm 2\mathrm{km}\cdot \mathrm{s}^{-1}$ in the 1445 Type-1 AGN in the subsample, still indicating (9 ± 3)% higher stellar velocity dispersions in Type-1 AGN. And the Students T-statistic technique is applied to determine the different mean values of $\log(\sigma)$ shown in Fig. 18 with confidence level higher than 10sigma between the Type-1 AGN and the Type-2 AGN.

It is hard to reasonably explain the statistically larger σ in Type-1 AGN than in Type-2 AGN, unless to assume that there were some lost Type-2 AGN with larger σ and/or assume that there were some lost Type-1 AGN with smaller σ. Larger σ commonly indicates stronger host galaxy contributions, indicating it is hard to miss Type-2 AGN with larger σ, due to their expected more apparent absorption features. Meanwhile, it could be expected to miss Type-1 AGN with smaller σ, due to weaker host galaxy contributions but stronger central AGN activities. The expected strong AGN activities can clearly lead the lost Type-1 AGN with smaller intrinsic σ to be a true Type-1 AGN but without measured stellar velocity dispersions, quite similar as the Type-1 AGN without measured σ in the parent sample. As discussed results in subsection 4.3, the Type-1 AGN without measured σ could have statistically larger (at least not smaller) σ than the Type-1 AGN with well measured σ. Therefore, statistically larger σ is robust enough in Type-1 AGN than in Type-2 AGN.

Before the end of the subsection, three points are noted. First, effects of different aperture sizes are not considered on measured σ, because the same effects can be confirmed for the 1445 Type-1 AGN and the 1445 Type-2 AGN in the subsamples with the same redshift distributions, indicating few effects of different aperture sizes on the results shown in Fig. 18. Second, effects of host galaxy morphologies (including contributions of bars and/or disks of host galaxies) are not considered on the measured σ, because barred galaxies, unbarred galaxies, merging galaxies, and those hosting pseudo-bulges do not represent outliers in $M_{\mathrm{BH}} - \sigma$ relations as discussed in more recent Bennert et al. (2015, 2021) and as shown results in Batiste et al. (2017). Third, effects of inclination are not considered on the measured stellar velocity dispersions. As discussed in Bellovary et al. (2014) and then followed in Sexton et al. (2019), there are apparent effects of galaxy orientation on measured stellar velocity dispersions, due to contributions of disk rotating components. However,

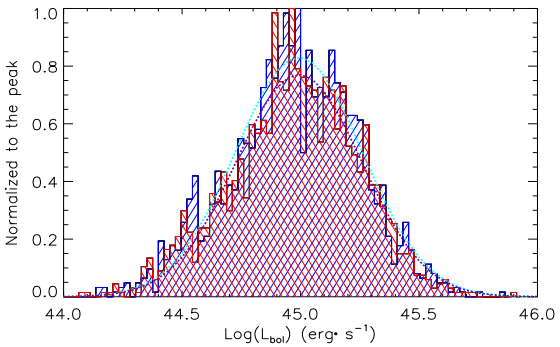

Figure 19. Bolometric luminosity distributions of the 1445 Type-1 AGN (histogram filled by blue lines) and the 1445 Type-2 AGN (histogram filled by red lines) in the subsamples, which have the same distributions of z, O3HB, N2HA and L_{O3}. Dashed lines in purple and in cyan represent the corresponding best fitting Gaussian profiles for the distributions of the Type-2 AGN and of the Type-1 AGN, respectively.

more recently, from a Hubble Space Telescope snapshot imaging survey, Kim et al. (2021) have shown[5] that Type-1 and Type-2 AGN are almost indistinguishable in terms of their Hubble type distributions, through Swift-BAT unbiased X-ray selected AGN with redshift smaller than 0.1 and with bolometric luminosity around 10^{43-46}erg $\cdot$ s^{-2}. Based on the reported luminosity L_{o3} of core components of [O III] lines of the AGN in the subsamples, the bolometric luminosities $L_{bol} \sim 10 \times L_{5100\text{Å}}$ (Richards et al. 2006; Duras et al. 2020; Netzer 2020) can be estimated by the reported correlation between continuum luminosity $L_{5100\text{Å}}$ and L_{o3} in Zhang et al. (2017), and shown in Fig. 19 for the Type-1 AGN and Type-2 AGN in the subsamples, which are well comparable to the bolometric luminosities of AGN in Kim et al. (2021). Therefore, considering the results in Kim et al. (2021) that there is negligible difference in terms of Hubble type between Type-1 and Type-2 AGN, there are no statistical inclination effects on our final stellar velocity dispersion comparisons between Type-1 AGN and Type-2 AGN in the manuscript.

Based on the results above, statistically larger σ can be well confirmed in the Type-1 AGN than in the Type-2 AGN with significance level higher than 10sigma, after considerations of necessary effects. Therefore, unless there was stable evidence to support different $M_{\rm BH} - \sigma$ relations applied to determine central BH masses or to support quite different evolution histories in Type-1 AGN and in Type-2 AGN, larger stellar velocity dispersions in the Type-1 AGN than in the Type-2 AGN leads to an interesting challenge to the Unified Model of AGN.

[5] In 2018, Bornancini & Garcia Lambas (2018) have shown that host galaxies of the majority of Type 1 AGN are elliptical and/or compact galaxies, while host galaxies of Type 2 AGN present more scatters, but through samples of high redshift Type-1 AGN and Type-2 AGN with redshift larger than 0.3 and smaller than 1.1. Therefore, in the manuscript, results in Kim et al. (2021) for low redshift AGN are preferred and mainly considered.

6. SUMMARIES AND CONCLUSIONS

The main summaries and conclusions are as follows.

- So-far the largest sample of 6260 low redshift Type-1 AGN ($z < 0.3$), about 85 times larger than the more recent sample of Type-1 AGN with measured spatially resolved stellar velocity dispersions σ_{bt} in Bennert et al. (2015, 2021), have their stellar velocity dispersions σ measured through absorption features around 4000Å. And the measured σ are well consistent with the σ_{bt} for the Type-1 AGN with apparent absorption features around 4000Å.

- Meanwhile, almost all the low redshift Type-2 AGN ($z < 0.3$) in SDSS DR12 have the stellar velocity dispersions σ measured through absorption features around 4000Å. And the measured σ are well consistent with the SDSS provided dispersions of the Type-2 AGN.

- Based on series of artificial spectra created by Type-2 AGN spectrum plus contributions from both AGN continuum emissions and broad line emissions, contributions from both AGN continuum emissions and broad line emissions can also lead to reliable measured stellar velocity dispersions through the absorption features around 4000Å, however, strong AGN continuum emissions can lead to part of Type-1 AGN of which stellar velocity dispersions cannot be measured, and lead to the measured stellar velocity dispersions about 4% higher than the intrinsic values.

- Although half of low redshift Type-1 AGN, about 6082 Type-1 AGN, have not apparent absorption features around 4000Å , leading the half of low redshift Type-1 AGN without measured stellar velocity dispersions, properties of the mean spectra of the 6260 Type-1 AGN with measured σ and the 6082 Type-1 AGN without measured σ can be applied to confirm that the 6082 Type-1 AGN without measured σ are mainly due to weak absorption features overwhelmed in the emission features of central AGN activities.

- Based on the positive correlation between σ and [O III] line luminosity, the half of low redshift Type-1 AGN without apparent absorption features around 4000Å should have intrinsic stellar velocity dispersions statistically larger (at least not smaller) than the 6260 Type-1 AGN with measured stellar velocity dispersions, due to statistically higher [O III] line lumi-

nosities of the half of low redshift Type-1 AGN without apparent absorption features around 4000Å.

- Based on the measured stellar velocity dispersions σ of the largest sample of Type-1 AGN and the largest sample of Type-2 AGN in SDSS DR12, direct σ comparisons can lead to statistically larger σ in the Type-1 AGN than in the Type-2 AGN, without considerations of necessary further effects.

- Even after considering necessary effects of different evolution histories and central AGN activities on direct σ comparisons between Type-1 AGN and Type-2 AGN, such as the effects of different redshift, different [O III] line luminosities of core components and different narrow line ratios of O3HB and N2HA, statistically $(9 \pm 3)\%$ larger σ can be well confirmed in the Type-1 AGN than in the Type-2 AGN with significance level higher than 10sigma.

- Unless there was strong evidence to support different $M_{\rm BH} - \sigma$ relations or to support quite different evolution histories between Type-1 AGN and Type-2 AGN, the statistically larger σ in Type-1 AGN provides an interesting but strong challenge to the Unified model of AGN.

ACKNOWLEDGEMENTS

Zhang gratefully acknowledge the anonymous referee for giving us constructive comments and suggestions to greatly improve the paper. Zhang gratefully thanks the kind financial support from Nanjing Normal University and the kind grant support from NSFC-12173020. This manuscript has made use of the data from the SDSS projects. The SDSS-III web site is http://www.sdss3.org/. SDSS-III is managed by the Astrophysical Research Consortium for the Participating Institutions of the SDSS-III Collaborations. The manuscript has made use of the data from the Indo-U.S. Coude Feed Spectral Library (https://www.noao.edu/cflib/) which consists of spectra for 1273 stars obtained with the 0.9m Coude Feed telescope at Kitt Peak National Observatory.

REFERENCES

Alam, S., et al., 2015, ApJS, 219, 12

Antonucci, R., 1993, ARA&A, 31, 473

Baldwin, J. A.; Phillips, M. M.; Terlevich, R. 1981, PASP, 93, 5

Balokovic, M.; Brightman, M. ; Harrison, F. A.; et al., 2018, ApJ, 854, 42

Barth, A. J.; Ho, L. C.; Sargent, W. L. W., 2002, AJ, 124, 2607

Barth, A. J.; Greene, J. E.; Ho, L. C., 2005, ApJL, 619, 151

Barth, A. J.; Bennert, V. N.; Canalizo, G., et al., 2015, ApJS, 217, 26

Batiste, M.; Bentz, M. C.; Raimundo, S. I.; Vestergaard, M.; Onken, C. A., 2017, ApJL, 838, 10

Bellovary, J. M.; Holley-Bockelmann, K.; Gultekin, K.; et al., 2014, MNRAS, 445, 2667

Bennert, V. N., Treu, T.; Auger, M. W.; et al., 2015, ApJ, 809, 20

Bennert, V. N.; Loveland, D.; Donohue, E.; et al., 2018, MNRAS, 481, 138

Bennert, V. N.; Treu, T.; Ding, X.; et al., 2021, ApJ, 921, 36

Bentz, M. C.; Walsh, J. L.; Barth, A. J., et al., 2010, ApJ, 716, 993

Bentz, M. C., et al., 2013, ApJ, 767, 149

Bianchi, S.; Maiolino, R.; Risaliti, G., 2012, Advances in Astronomy, 2012, 17

Blandford, R. D.; McKee, C. F., 1982, ApJ, 255, 419

Bornancini, C.; Garcia Lambas, D., 2018, MNRAS, 479, 2308

Bornancini, C.; Garcia Lambas, D., 2020, MNRAS, 494, 1189

Brewer, B. J. ; Treu, T.; Pancoast, A.; et al., 2011, ApJL, 733, 33

Brown, A.; Nayyeri, H.; Cooray, A.; Ma, J.; Hickox, R. C.; Azadi, M, 2019, ApJ, 871, 87

Bruzual, G.; Charlot, S. 2003, MNRAS, 344, 1000

Cappellari, M., 2017, MNRAS, 466, 798

Cid Fernandes, R.; Mateus, A.; Sodre, L.; Stasinska, G.; Gomes, J. M., 2005, MNRAS, 358, 363

Duras, F., Bongiorno, A., Ricci, F., et al. 2020, A&A, 636, 73

Ferrarese, F.; Merritt, D., 2000, ApJL, 539, 9

Franceschini, A.; Braito, V.; Fadda, D., 2002, MNRAS Letter, 335, 51

Gebhardt, K., et al., 2000, ApJL, 539, 13

Graham, A. W., Onken, C. A., Athanassoula, E., Combes, F. 2011, MNRAS, 412, 2211

Greene, J. E.; Ho, L. C., 2005, ApJ, 627, 721

Greene, J. E.; Ho, L. C., 2005, ApJ, 630, 122

Greene, J. E.; Ho, L. C., 2006, ApJ, 641, 117

Grier, C. J.; Trump, J. R.; Shen, Y.; et al., 2017, ApJ, 851, 21

Harris, C. E.; Bennert, V. N.; Auger, M. W.; Treu, T.; Woo, J.-H.; Malkan, M. A., 2012, ApJS, 201, 29

Heisler, C. A.; Lumsden, S. L.; Bailey, J. A., 1997, Nature, 385, 700

Hiner, K. D., et al., 2009, ApJ, 706, 508

Ho, L. C.; Kim, M.-J., 2014, ApJ, 789, 17

Kaspi, S., et al., 2000, ApJ, 533, 631

Kauffmann, G.; Heckman, T. M. ; White, S. D. M.; et al., 2003a, MNRAS, 341, 33

Kauffmann, G., et al. 2003, MNRAS, 346, 1055

Table 1. Parameters of the 1445 Type-1 AGN in the subsample

mpf	z	σ	L_{O3}	O3HB	N2HA	mpf	z	σ	L_{O3}	O3HB	N2HA
0266-51602-0239	0.063	106±11	40.22	0.705	-0.33	0267-51608-0300	0.067	99±13	40.32	0.583	-0.03
0270-51909-0266	0.110	124±13	41.06	1.045	-0.11	0270-51909-0429	0.128	83±14	39.87	0.104	-0.29
0271-51883-0200	0.061	140±9	40.57	0.929	0.162	0271-51883-0322	0.086	140±9	41.10	1.032	0.181
0272-51941-0329	0.078	135±10	41.21	0.936	-0.01	0273-51957-0460	0.096	131±15	41.28	1.013	0.005
0273-51957-0579	0.131	238±22	41.91	1.072	0.022	0274-51913-0141	0.138	111±10	41.28	0.988	0.098

NOTE— The first column and the seventh column show the information of SDSS PLATE-MJD-FIBERID. The second column and the eighth column show the redshift. The third column and the ninth column show the measured σ in the unit of km $\cdot$ s^{-1} through the absorption features around 4000Å. The fourth column and the tenth column show the $\log(L_{O3})$ of the core components of [O III]λ5007Å in the unit of erg $\cdot$ s^{-1}. The fifth column and the eleventh column show the $\log(O3HB)$. The sixth and twelfth columns show the $\log(N2HA)$.

Table 1 is published in its entirety in the machine-readable format.

Table 2. Parameters of the 1445 Type-2 AGN in the subsample

mpf	z	σ	L_{O3}	O3HB	N2HA	mpf	z	σ	L_{O3}	O3HB	N2HA
0266-51630-0147	0.030	99±7	39.92	1.007	-0.05	0266-51630-0392	0.122	124±18	41.21	0.571	-0.04
0269-51910-0105	0.184	126±21	40.75	0.531	-0.04	0269-51910-0168	0.176	131±21	40.78	0.889	-0.03
0271-51883-0178	0.181	124±15	41.76	0.814	-0.19	0272-51941-0529	0.177	208±24	40.91	0.871	-0.04
0274-51913-0115	0.095	107±10	40.38	0.633	-0.24	0274-51913-0230	0.077	115±7	41.19	0.650	-0.24
0275-51910-0438	0.150	92±12	41.27	0.681	-0.15	0276-51909-0147	0.108	117±18	40.12	0.443	-0.29

NOTE—The first column and the seventh column show the information of SDSS PLATE-MJD-FIBERID. The second column and the eighth column show the redshift. The third column and the ninth column show the measured σ in the unit of km $\cdot$ s^{-1} through the absorption features around 4000Å. The fourth column and the tenth column show the $\log(L_{O3})$ of the core components of [O III]λ5007Å in the unit of erg $\cdot$ s^{-1}. The fifth column and the eleventh column show the $\log(O3HB)$. The sixth and twelfth columns show the $\log(N2HA)$.

Table 2 is published in its entirety in the machine-readable format.

Kewley, L. J.; Dopita, M. A.; Sutherland, R. S.; Heisler, C. A.; Trevena, J. 2001, ApJ, 556, 121

Kewley, L. J.; Groves, B.; Kauffmann, G.; Heckman, T., 2006, MNRAS, 372, 961

Kewley, L. J.; Nicholls, D. C.; Sutherland, R. S., 2019, ARA&A, 57, 511

Kim, M.; Barth, A. J.; Ho, L. C.; Son, S., 2021, ApJS, 256, 40

Komossa, S. ; Xu, D., 2007, ApJL, 667, 33

Kormendy, J.; Ho, L. C., 2013, ARA&A, 51, 511

Kovacevic, J.; Popovic, L. C.; Dimitrijevic, M. S., 2010, ApJS, 189, 15

Kuraszkiewicz, J.; Wilkes, B. J.; Atanas, A.; et al., 2021, ApJ, 913, 134

Lyke, B. W.; Higley, A. N.; McLane, J. N.; et al., 2020, ApJS, 250, 8

Marinucci, A.; Bianchi, S.; Nicastro, F.; Matt, G.; Goulding, A. D., 2012, ApJ, 748, 130

Mateos, S., et al., 2016, ApJ, 819, 166

McConnell, N. J.; Ma, C. P., 2013, ApJ, 764, 184

Miller, J. S.; Goodrich, R. W., 1990, ApJ, 355, 456

Moran, E. C.; Barth, A. J.; Kay, L. E.; Filippenko, A. V., 2020, ApJL, 540, 73

Nagao, T., et al., 2004, AJ, 128, 109

Nelson, C. H.; Whittle, M., 1996, ApJ, 465, 96

Nelson, C. H., 2000, ApJL, 544, 91

Netzer, H., 2009, ApJ, 695, 793

Netzer, H., 2015, ARA&A, 53, 365

Netzer, H. 2020, MNRAS, 488, 5185

Oh, K., et al., 2015, ApJS, 219, 1

Onken, C. A.; Ferrarese, L.; Merritt, D.; Peterson, B. M.; Pogge, R. W.; Vestergaard, M.; Wandel, A., 2004, ApJ, 615, 645

Onori, F.; Ricci, F.; La Franca, F.; et al., 2017, MNRAS Letter, 468, 97

Pancoast, A.; Brewer, B. J.; Treu, T.; Park, D.; Barth, A. J.; Bentz, M. C.; Woo, J.-H., 2014, MNRAS, 445, 3073

Park, D.; Kelly, B. C.; Woo, J.-H.; Treu, T., 2012, ApJS, 203, 6

Peterson, B. M., et al., 2004, ApJ, 613, 682

Peters, C. M.; Richards, G. T.; Myers, A. D.; et al., 2015, ApJ, 811, 95
Prugniel, Ph.; Soubiran, C., 2001, A&A, 369, 1048
Rafiee, A.; Hall, P. B., 2011, ApJS, 194, 42
Rakshit, S.; Stalin, C. S.; Chand, H.; Zhang, X. G., 2017, ApJS, 229, 39
Richards, G. T., et al., 2002, AJ, 123, 2945
Richards, G. T., Lacy, M., Storrie-Lombardi, L. J., et al. 2006, ApJS, 166, 470
Rix, H.-W.; White, S. D. M., 1992, MNRAS, 254, 389
Ross, N. P.; et al., 2012, ApJS, 199, 3
Savorgnan, G. A. D.; Graham, A. W., 2015, MNRAS, 446, 2330
Savic, D.; Goosmann, R.; Popovic, L. C.; Marin, F.; Afanasiev, V. L., 2018, A&A, 614, 120
Shen, Y.; Richards, G. T.; Strauss, M. A., et al., 2011, ApJS, 194,
Shen, Y.; Brandt, W. N.; Dawson, K. S.; ET AL., 2015a, ApJS, 2015a, 216, 4
Shen, Y.; Greene, J. E.; Luis C. Ho, L. C.; et al., 2015b, ApJ, 805, 96
Shu, Y.; Bolton, A. S.; Schlegel, D. J.; et al., 2012, AJ, 143, 90
Siebenmorgen, R.; Haas, M.; Krugel, E.; Schulz, B., 2005, A&A, 436, 5
Sexton, R. O.; Canalizo, G.; Hiner, K. D.; et al., 2019, ApJ, 878, 101
Tran, H. D., 2003, ApJ, 583, 632
Thomas, D.; Steele, O.; Maraston, C.; et al., 2013, MNRAS, 431, 1383
Tremaine, S.; Gebhardt, K.; Bender, R.; et al., 2002, ApJ, 574, 740
Valdes, F.; Gupta, R.; Rose, J. A.; Singh, H. P.; Bell, D. J., 2004, ApJS, 152, 251
Villarroel, B.; Korn, A. J., 2014, Nature Physics, 10, 417
Vestergaard, M., 2002, ApJ, 571, 733
Williams, P. R.; Pancoast, A.; Treu, T., et al., 2018, ApJ, 866, 75
Woo, J.-H.; Treu, T.; Barth, A. J.; et al., 2010, ApJ, 716, 269
Woo, J.-H., et al., 2013, ApJ, 772, 49
Woo, J.-H.; Yoon, Y.; Park, S.; Park, D.; Kim, S. C., 2015, ApJ, 801, 38
Woo, J.-H.; Bae, H. J.; Son, D.; Karouzos, M., 2016, ApJ, 817, 108
Vanden Berk D. E., et al., 2001, AJ, 122, 549
Xiao, T.; Barth, A.; Greene, J. E.; Ho, L. C.; Bentz, M. C.; Ludwig, R. R., Jiang Y., 2011, ApJ, 739, 28
Zhang, X. G., 2014, MNRAS, 438, 557
Zhang, X. G.; Feng, L., 2016, MNRAS, 457, 3878
Zhang, X. G.; Feng, L., 2017, MNRAS, 468, 620
Zhang, X. G.; Bao M.; Yuan, Q., 2019, MNRAS Letter, 490, 81
Zhang, X. G.; Feng Y.; Chen, H.; Yuan, Q., 2020, ApJ, 905, 97
Zhang, X. G., 2021, MNRAS, 502, 2508
Zhang, X. G., 2021a, ApJ, 909, 16, ArXiv:2101.02465
Zhang, X. G., 2021b, ApJ accepted, ArXiv:2107.09214
Zhang, X. G., 2021c, MNRAS accepted, ArXiv:2108.09714
Zou, F.; Yang, G.; Brandt, W. N.; Xue, Y., 2019, ApJ, 878, 11